Interactions between Lightning and Ship Traffic

Michael Jay Peterson[1]

[1]ISR-2, Los Alamos National Laboratory

March 13, 2023

Abstract

It is important to understand connections between society and the natural environment for anticipating environmental hazards and anthropogenic effects on the broader Earth system. In this study, we conduct a detailed exploration of the interactions between oceanic thunderstorms and maritime traffic. Shipping traffic produces aerosols that perturb the otherwise "clean" ocean environment. Prior work proposed these aerosol effects as the cause of increased lightning activity over certain shipping lanes. However, introducing tall well-grounded objects into a high electric field environment might also facilitate lightning discharges, as we see with upward lightning over land. We consider both possibilities in this work.

Our analyses of the thunderstorms responsible for the enhanced lightning activity over the shipping lane with the clearest anthropogenic signal indicate that the anthropogenic signature results from an increased frequency of lightning-producing storms. We did not find evidence of variations in the microphysical parameters describing the storms over shipping lanes and other nearby oceanic regions that might suggest aerosol effects. In contrast, matching lightning stroke data with ship transponder events in oceanic regions where public data are available reveals a strong signal from direct ship interactions with lightning that results in a 1-2 orders of magnitude increase in stroke frequency at current ship locations compared to other nearby regions. These results highlight the central role of direct ship interactions in explaining lightning enhancements over shipping lanes.

We also document the frequency of these direct lightning interactions across various categories of vessels and on individual ships present in the public data.

Interactions between Lightning and Ship Traffic

Michael Peterson[1]

[1] ISR-2, Los Alamos National Laboratory, Los Alamos, New Mexico

Corresponding author: Michael Peterson (mpeterson@lanl.gov)

Key Points:

- Lightning enhancements over shipping lanes are accompanied by increased thunderstorm activity without clear evidence of storm invigoration
- Lightning over maritime routes preferentially occurs close to current ship positions compared to other nearby locations surrounding the ship
- Direct ship interactions, aerosol effects, and local weather patterns are all important for understanding lightning enhancements

LA-UR-23-20031

Abstract

It is important to understand connections between society and the natural environment for anticipating environmental hazards and anthropogenic effects on the broader Earth system. In this study, we conduct a detailed exploration of the interactions between oceanic thunderstorms and maritime traffic. Shipping traffic produces aerosols that perturb the otherwise "clean" ocean environment. Prior work proposed these aerosol effects as the cause of increased lightning activity over certain shipping lanes. However, introducing tall well-grounded objects into a high electric field environment might also facilitate lightning discharges, as we see with upward lightning over land. We consider both possibilities in this work.

Our analyses of the thunderstorms responsible for the enhanced lightning activity over the shipping lane with the clearest anthropogenic signal indicate that the anthropogenic signature results from an increased frequency of lightning-producing storms. We did not find evidence of variations in the microphysical parameters describing the storms over shipping lanes and other nearby oceanic regions that might suggest aerosol effects. In contrast, matching lightning stroke data with ship transponder events in oceanic regions where public data are available reveals a strong signal from direct ship interactions with lightning that results in a 1-2 orders of magnitude increase in stroke frequency at current ship locations compared to other nearby regions. These results highlight the central role of direct ship interactions in explaining lightning enhancements over shipping lanes.

We also document the frequency of these direct lightning interactions across various categories of vessels and on individual ships present in the public data.

Plain Language Summary

It was previously shown that there is more lightning over certain shipping lanes compared to the surrounding oceans. These enhancements were attributed to pollution from shipping traffic making it easier for thunderstorms to form. However, tall objects in high electric field environments are also known to initiate lightning. An alternate explanation for the lightning enhancement is that tall well-grounded ships may be facilitating lightning production – particularly in storms that are near the tipping point between remaining Electrified Shower Clouds (ESCs) and becoming thunderstorms.

Our analyses indicate that there are no clear differences in the thunderstorms responsible for the lightning enhancement that would suggest aerosol effects. There are simply more thunderstorms over the shipping lane compared to the nearby oceanic regions, supporting the tipping point explanation. Moreover, directly matching lightning strokes with ship positions provides clear evidence of lightning enhancements specifically at the ship location from direct interactions with the vessel.

1 Introduction

Interactions between ships and atmospheric electricity have been observed for thousands of years. Some of the first recorded descriptions of corona discharges (Aleksandrov et al., 2002; Arcanjo et al., 2021) are found in sources from antiquity. In his A.D. 77 work "Historia Naturalis," Pliny the Elder described the phenomenon, which he attributes to the Roman gods

Castor and Pollox: “I have seen, during the night-watches of the soldiers, a luminous appearance, like a star, attached to the javelins on the ramparts. They also settle on the yardarms and other parts of ships while sailing, producing a kind of vocal sound, like that of birds flitting about. When they occur singly they are mischievous, so as even to sink the vessels, and if they strike on the lower part of the keel, setting them on fire” (Plinius, 77). This phenomenon would only later come to be known by its modern common name of St Elmo’s fire – named for St. Erasmus, who like Castor and Pollox, was credited with protecting sailors from harm – and studied using modern measurements and scientific methods (Whipple and Scrase, 1936; Cockbain, 1945; Lundquist, 1985; Wescott 1996).

While many of the observations in Historia Naturalis have not held up to millennia of scientific scrutiny, the key observables in Pliny’s description – occurring on pointed objects, the characteristic hissing sound, and the concerns over atmospheric electrical phenomena igniting fires on ships at sea – are consistent with our modern understanding of corona discharges and the lightning strikes sometimes associated with them (Aleksandrov et al., 2001; Bazelyan et al., 2008; Wu et al., 2017). Later histories are filled with reports of lightning strikes on ships at sea. Slow sailing speeds and being the only tall object around for many kilometers leaves ships particularly exposed when lightning hazards manifest. Reports of the damage sustained by sailing ships in logs and journal articles (Priestley, 1775; Lightning, 1840; Ship destroyed, 1846) range from shrapnel injuries and repairable damage to the mast to compass failures hindering navigation, and even fires resulting in the complete loss of the vessel.

Following Benjamin Franklin’s lightning experiments, his British colleague Dr. William Watson petitioned the Royal Navy to install lightning protection systems on their ships. The proposed early systems consisted of a brass wire connecting the top of the mast to the sea surface. The Royal Navy ultimately favored a different design whose complexity and difficulty to deploy (it could not be used permanently as it interfered with the riggings) limited its success (Bernstein and Reynolds, 1978). Maritime lightning protection systems have improved over the centuries, but still conform to the same basic principle of providing conductive paths from potential attachment points to ground that should not result in damage to the vessel or harm to its occupants.

While we know that lightning impacts oceangoing vessels, it is not clear how often this occurs, or whether certain types of vessels are more susceptible to lightning strikes than others. Moreover, historic levels of global shipping activity in recent decades are expected to cause anthropogenic changes to the otherwise clean ocean environments that are critical for the Earth system. The two major anthropogenic effects that have been proposed are aerosol effects on thunderstorm development from burning fuel and direct lightning interactions with ships, though the former has been prioritized over the latter in prior studies.

Effects of the aerosols from ship exhaust on the ocean environment have been noted since the dawn of the satellite era. “Anomalous cloud lines” were reported over the ocean in early satellite imagery from the Television InfraRed Observation Satellite (TIROS-VII) that extended 500 km in length and 25 km in width (Conover, 1966). As these clouds were linked to shipping traffic, they came to be known as “ship track” clouds. Oceanic environments are described as “clean” for having small numbers of aerosols compared to land. These aerosols act as cloud condensation nuclei (CCNs), and their scarcity results in low maritime clouds containing smaller numbers of large precipitation droplets (O'Dowd et al., 1997; Han et al. 1998; Capaldo et al., 1999; Schreier et al., 2007). Pollution from shipping exhaust introduces aerosols into these clean regions, facilitating cloud growth to produce the ship track signature along the sea lanes.

Thornton et al. (2017) found a similar ship track signature in two major shipping lanes within the global lightning data provided by the World Wide Lightning Location Network (WWLLN). They attribute the enhanced oceanic lightning activity at the boundary between the Bay of Bengal and the Indian ocean and in the South China Sea between Vietnam and Malaysia solely to aerosol effects from shipping traffic through the Strait of Malacca and the port of Singapore. They suggest that shipping aerosols are not only responsible for low (< 2 km) ship track clouds, but also invigorate deep convection and increase electrification over the shipping lanes.

At the same time, the mere presence of a grounded tall ship on an otherwise flat ocean surface might be sufficient to cause a notable increase in the lightning stroke rates measured by WWLLN. Lightning strikes on tall objects are relatively common over land (Aleksandrov et al., 2005) and can either be self-triggered or triggered by an ongoing lightning flash (Wang and Takagi, 2012; Warner et al., 2014; Montoya et al., 2014; Schumann et a., 2019). They are particularly common in the electrified stratiform regions of Mesoscale Convective Systems (MCSs) where the lack of a vigorous updraft allows charged hydrometeors to accumulate in horizontally-extensive vertically stacked layers over long periods of time between successive flashes (Stolzenburg et al., 1994; Carey et al., 2005). These meteorological conditions are also present in maritime storms and explain why oceanic thunderstorms typically generate stronger conduction currents than land storms despite producing lower flash rates (Mach et al., 2011). Introducing a preferential path to ground into such an environment might facilitate the transition of borderline Electrified Shower Clouds (ESCs) - that have strong electric fields but have not produced lightning - into thunderstorms that are detectable by WWLLN.

In this study, we take a detailed look at the data that supports either of these possible anthropogenic impacts of naval traffic on the Earth system. We then use the data to comment on how each effect might explain the observed lightning trends. Finally, we elaborate on the vessels that have frequent lightning interactions for the first time.

2 Data and Methods

We employ a diverse collection of lightning, shipping, and thunderstorm microphysical observations in this study that do not share a common domain. Our selection of these disparate datasets is motivated by two factors: (1) independent evaluation of the same research-grade datasets from prior studies for reproducibility and (2) prioritizing the use of public data over commercial datasets that are generally not available for research purposes. In each analysis, we will make use of the longest possible data record given the mis-matched domains of the underlying observations to generate robust statistical descriptions of the lightning and thunderstorm trends. The particularities of these datasets, including their spatial and temporal domains, are documented in the following sections.

2.1 The World Wide Lightning Location Network

For consistency with past studies, we will use WWLLN stroke data to examine the lightning that occurs over shipping lanes. More accurate datasets exist (i.e, Thomas et al., 2004), but these measurements lack the global coverage and long historical record of WWLLN. If WWLLN detects a trend related to ship interactions, then it would only be more accurately resolved using a different lightning network.

WWLLN uses Very Low Frequency (VLF: 3-30 kHz) band radio receivers scattered across the globe to detect and geolocate lightning (Lay et al., 2004; Rodger et al., 2006; Abarca et al., 2010; Hutchins et al., 2012; Jacobson et al., 2006). The VLF pulse emitted by a lightning stroke propagates from the source to the sensor within the Earth-ionosphere waveguide over potentially thousands of kilometers with reduced attenuation compared to higher frequencies. Removing the line-of-sight detection requirement allows systems like WWLLN to achieve global coverage at minimal cost using only dozens of well-sited sensors (Jacobson et al., 2006). When at least five stations detect the same lightning signal (or, “sferic”), the Time of Group Arrival (TOGA) is extracted from the waveform data at each station, and this information is used to calculate the location of the lightning source on the Earth.

The accuracy of WWLLN geolocation solutions has been quantified relative to multiple lightning detection networks, and has changed over time as the WWLLN network grew and its location algorithm was refined. The current average location accuracy is thought to be within 10 km of the source based on comparisons with the National Lightning Detection Network (NLDN: Cummins et al., 2009), which includes a < 5 km systematic offset in the detections over the continental United States (Abarca et al., 2010). As this is a climatological average, WWLLN geolocation performance may be better or worse for the strokes from an individual thunderstorm or different locations on Earth. Our results in Section 3 suggest that the recent (since 2019) WWLLN location accuracy for oceanic strokes is < 2 km with no systematic offset.

The WWLLN data product only reports the locations and times of individual strokes. Unlike other lightning sensors, WWLLN does not attempt to cluster these strokes into features representing distinct lightning flashes or thunderstorms. Therefore, we create our own WWLLN “thunderstorm area” dataset based on the approach used by NASA’s Lightning Imaging Sensor (LIS: Christian, 1994; Mach et al., 2007). WWLLN strokes are assigned to the same thunderstorm if they occur in close spatiotemporal proximity to one another. We loop through the WWLLN strokes, identifying events that satisfy a 3-termed Weighted Euclidian Distance (WED) model consisting of longitude (X), latitude (Y), and time (T) with thresholds of 0.5 degrees in X and Y and 30 minutes in T. These thresholds are largely arbitrary beyond exceeding typical time and spatial scales for the convective thunderstorms detected by WWLLN. Due to the large volume of WWLLN strokes, we also do not convert geographic coordinates into distances to avoid the increased computational expense. Note that these thresholds are far more generous than LIS, which used a 16.5 km distance threshold and an implicit time threshold equal to the minute-scale view time of the instrument while it was over a given storm.

2.2 Tropical Rainfall Measuring Mission (TRMM) Data

We will compare our WWLLN thunderstorm area feature statistics in the Bay of Bengal region with Precipitation Radar (PR: Kozu et al., 2001; Kummerow et al., 1998) profiles and storm feature statistics from the Tropical Rainfall Measuring Mission (TRMM) satellite. TRMM provided snapshots of global storms from between 1998 and 2015, though we avoid using the 2015 data due to orbital decay. The PR recorded three-dimensional reflectivity data over a 215 km swath with pixels (at nadir) spanning 4.3 km in the horizontal direction and 0.25 km in the vertical. The PR swath width and horizontal pixel size increased slightly after the August 2001 satellite boost to a higher orbit to conserve fuel and prolong the mission (Kozu et al., 2001).

The PR reflectivity profile data used in Thornton et al., (2017) are one of the simplest derived PR data products. Raining pixels are identified in the PR swath data, and then the vertical reflectivity data are extracted from each of these pixels. The key limitation of the profile data is that each profile does not represent an independent storm. A single storm spanning multiple pixels across the PR swath will contribute multiple profiles, and this can introduce bias from larger storms – particularly those that occur in regions with infrequent storm activity.

To counteract these biases, the PR data needs to be clustered into distinct storm features, similar to our WWLLN area thunderstorm features. TRMM Radar Precipitation Features (RPFs: Liu et al., 2008) cluster contiguous regions of raining pixels across the PR swath into features representing independent raining areas. Each feature additionally contains information gathered from the full suite of sensors on the TRMM satellite - the Visible and Infrared Scanner (VIRS), the TRMM Microwave Imager (TMI), the PR, and the LIS. We also evaluate RPF properties over the Bay of Bengal shipping lane.

2.3 Automatic Identification System (AIS) Data

Ship locations are provided by Automatic Identification System (AIS) transponders. The AIS system reports information about each vessel, including its position, to coastal authorities and to nearby vessels for collision avoidance. The International Marine Organization (IMO) requires all ships in certain classes of activity (i.e., all ships on international voyages in excess of 300 gross tonnes, all other cargo ships in excess of 500 gross tonnes, and all passenger ships) to be fitted with an AIS transponder and for it to be active at all times (with certain exceptions) (International Maritime Organization, 2019). It is important to note that activities where AIS use is not mandated – including domestic shipping – account for a large volume of maritime activity that may still contribute to lightning enhancements in the WWLLN data.

Global AIS databases are generated by commercial organizations who sell the data for profit. Event data are generally not provided by these companies for use in research. Acquiring the Bay of Bengal shipping data proved to be prohibitively costly for this study. However, regional AIS event datasets are also produced by individual nations' coastal authorities. The largest of these datasets is available publicly from NOAA, and includes robust – though incomplete – AIS data from the territorial waters of the United States and nearby oceans.

We acquired the NOAA Office for Coastal Management's complete AIS dataset from (NOAA, 2022) from between 1/1/2019 and 12/31/2021, and matched the AIS events to WWLLN strokes using generous thresholds to capture all lightning activity in the vicinity of maritime traffic. For each WWLLN stroke, we searched the AIS database for all nearby ships that satisfied a second WED model with an X and Y threshold of 0.5 degrees and a T threshold of 10 minutes. We then recorded the number of nearby ships and the AIS information (i.e., identification information, position, length, heading, etc.) for the closest ship by distance. The differences in position between the stroke and the closest ship will allow us to seek evidence for WWLLN strokes occurring preferentially in close proximity to ships, while the ancillary AIS data provide context on the types of vessels that are prone to close lightning encounters.

2.4 The Emissions Database for Global Atmospheric Research (EDGAR)

As with Thornton et al. (2017), we compare the WWLLN data with shipping sector specific fine Particulate Matter ($PM_{2.5}$) emissions from the Emissions Database for Global Atmospheric Research (EDGAR: Olivier et al., 1994). EDGAR calculates shipping emissions by combining global AIS data with published information on ship emissions. The current version of EDGAR (v6.1: Crippa et al. 2019) differs from prior versions by updating all activity data up to the year 2018, and generating new shipping proxies and monthly profiles (Jalkanen et al., 2012; Johansson et al., 2017), among other changes are not relevant to this study. We aggregate shipping emissions from 2003 to 2018 in our EDGAR analyses.

3 Results

To improve our understanding of lightning interactions with marine traffic, we will first revisit the prominent WWLLN signal over the shipping lane in the Bay of Bengal. Section 3.1 provides additional context for the results in Thornton et al. 2017 by analyzing the thunderstorms responsible for the lightning enhancements over the shipping lane - both using TRMM RPFs and WWLLN thunderstorm areas. We will then examine direct interactions between lightning and ship traffic using WWLLN strokes in the vicinity of AIS events in the NOAA dataset. Section 3.2 documents the frequency of WWLLN / AIS matches to constrain the magnitude of lightning enhancements that can be attributed to direct ship interactions. Section 3.3, then, documents the vessels that have frequent interactions with lightning.

3.1 Enhanced Lightning Activity over the Bay of Bengal Shipping Lane

An important point of discussion from the original work on ship track clouds is that these clouds occur when the meteorological environment is already suitable for cloud production. The aerosol effects from ship exhaust modify cloud formation and growth, but we must recognize that complex atmospheric interactions external to aerosols are also key in their development. Similarly, we would not expect drastic lightning enhancements over all shipping lanes – only those with favorable conditions for thunderstorm development. We hypothesize that the most notable enhancements relative to the local background should occur in regions where local storms frequently approach the requirements for initiating lightning, and the presence of the shipping lane makes the difference between the storm remaining an ESC or becoming a thunderstorm. Note that this hypothesis does not consider the source of the lightning enhancement. Thornton et al. (2017) attributed lightning enhancements solely to aerosol effects. We consider both aerosol effects and direct lightning interactions with the ship as potential sources. If our hypothesis is valid, then we will see a notable increase in thunderstorm activity over the shipping lanes that is not accompanied by a significant difference in thunderstorm characteristics compared to nearby ocean regions.

Figure 1a uses the EDGAR shipping aerosol data from 2003 to 2018 to show the locations of the major shipping lanes across the Earth. Shipping routes extend between the major economic centers in the Americas, Europe, Africa, and Asia with the destinations, routes, and timetables determined by the business pressures involved in minimizing cost. The organization of global shipping infrastructure into specific origin and destination ports on each continent makes shipping routes predictable - particularly in regions where terrain features limit the number of efficient routes between ports, which can become problematic when unforeseen issues arise (Forti et al., 2021).

The shipping lanes that extend across the Bay of Bengal and the South China Sea examined by Thornton et al. (2017) produce a large amount of $PM_{2.5}$ emissions over a narrow width because they are located along the most efficient routes for both shipping traffic passing between Europe and Asia and petrochemical traffic moving from the Persian Gulf to Asia. In the Bay of Bengal, this traffic is forced south by the Indian and Sri Lankan landmasses but must progress northward to enter the natural choke point of the Straits of Malacca. The terrain constraints are removed in the South China Sea, allowing shipping traffic to spread out along the most efficient routes to reach each destination port, broadening the $PM_{2.5}$ emissions signal.

Global WWLLN strokes from 2005 to 2021 are shown in Figure 1b for comparison. Note that we have restricted the dynamic range of the color bar, as in Thornton et al. (2017). An unrestricted version of the plot is included as Supporting Information in Figure S1. Both segments of the shipping route show a pronounced increase in the local lightning frequency compared to adjacent oceanic regions whose peaks follow the maximum EDGAR $PM_{2.5}$ signature in Figure 1a, as reported by Thornton et al., (2017).

Before we zoom in to the Bay of Bengal shipping lane in subsequent analyses, it is important to appreciate the unique nature of this particular shipping route. The Bay of Bengal and the South China Sea are the only two regions in Figure 1 that exhibit an obvious signature of enhanced lightning over shipping lanes that cannot be otherwise accounted for via natural environmental effects. For example, there are large numbers of WWLLN strokes over the Atlantic Ocean east of the continental United States, and it is unclear whether there is an enhancement from the large volume of maritime traffic in this region beyond the natural contribution from the Gulf Stream. Moreover, the adjacent western segment of the shipping route between Europe and Asia that extends through the Red Sea, the Mediterranean Sea, and around the European landmass to ports in the North Sea has comparable EDGAR shipping emissions but no lightning enhancement visible in the WWLLN data.

The two shipping lanes in Asia discussed in Thornton et al. (2017) are unique, but it is unclear in the WWLLN stroke data whether their enhanced lightning signatures result from higher flash rates (indicating enhanced convective intensity) or a higher frequency of borderline ESCs over the shipping route becoming thunderstorms. To evaluate these possibilities, we turn to our WWLLN thunderstorm area data over the Bay of Bengal. Figure 2 shows the total EDGAR $PM_{2.5}$ emissions region (Figure 2a) along with the WWLLN thunderstorm area frequency (Figure 2b), the mean thunderstorm propagation distance (Figure 2c), and the mean number of WWLLN strokes per storm (Figure 2d). The region is divided into longitude bins, and the average amplitude of each parameter by latitude within the bin is overlaid with a solid white line plot. The broad domain in Figure 1a obscures much of the fine structure in the EDGAR emissions data. There are two peaks along the east-west shipping lane in Figure 2a (a primary northern peak and a weaker southern peak), as well as less-frequent and less-constrained maritime traffic throughout the region. The most prominent feature outside of the east-west shipping lane is the merging southwest-northeast route on the right side of the map from ships sailing around South Africa to reach the Straits of Malacca.

The enhanced lightning signature over the primary east-west shipping lane is also present in the thunderstorm area rates (Figure 2b). The peak (dashed) and 10%-10% latitude extent (dotted) of the EDGAR signal across longitude bins are fit to a linear model and overlaid as white lines in Figure 2b-d. The peak of the enhancement in thunderstorm frequency follows the EDGAR emissions peak along the shipping lane to the northeast, confirming the connection noted by Thornton et al. (2017). However, the attributes of WWLLN areas over the shipping lane do not appear to be distinct from thunderstorms in the nearby clean ocean regions. The mean thunderstorm propagation distances in Figure 2c are nearly identical to storms immediately to the south, and the only clear enhancements are far to the northwest over the Bay of Bengal. For all mapped regions, storms typically form and dissipate in the same approximate region – traveling over a distance that is smaller than the width of the ship track. The thunderstorm stroke rate data in Figure 2d, meanwhile, are dominated by random noise from a small sample size with no evidence of enhancement near the shipping lane.

The TRMM RPF characteristics likewise do not show evidence of notable enhancements over the shipping lane in the Bay of Bengal. Figure 3 plots four representative parameters in the same format as Figure 2: the unique RPF count (Figure 3a), the mean RPF minimum infrared brightness temperature (Figure 3b), the mean RPF passive microwave minimum 37 GHz Polarization Corrected Temperature (PCT) (Figure 3c), and the mean RPF PR echo top height (Figure 3). As in Thornton et al. (2017), we only show data from the winter months that have the strongest WWLLN signatures. The same plot for the full year is included as Figure S2. During this season, convection is only prevalent across the southern extent of the region with higher RPF rates and taller / more vigorous storms. The ship track is located near the gradient between frequent deep convection in the south and infrequent shallow convection in the north, and also passes close to apparent terrain effects in the east. The RPF minimum 37 GHz PCTs was selected because it showed the most complex behavior of available RPF parameters with a local minimum parallel to the ship track. However, its width is greater than the WWLLN signature and the minimum is two degrees further north than the EDGAR data. The poor match between these signatures makes it unlikely to be caused by the shipping lane. Instead, it emphasizes that local variations exist in this region beyond the absence / presence of ship traffic that need to be considered.

These TRMM results differ from the analyses presented in Thornton et al. (2017) because the past work did not account for these natural variations. Even the WWLLN signature in Figure 2b is inconsistent from west to east along the shipping lane. The eastern longitude bins closer to Sumatra and in the vicinity of the Andaman and Nicobar Islands have a broader WWLLN enhancement due to contributions from local terrain interactions. Meanwhile, the seasonal migration of the Intra Tropical Convergence Zone (ITCZ) and the onshore / offshore phases of the Indian monsoon introduce north-south variations that are nearly parallel to the ship track.

Using PR profile data to compare the winter only to the full year further emphasizes these natural variations in the data. Figure 4 shows vertical TRMM PR profiles in each latitude bin across the domain mapped in Figure 2. Mean reflectivity profiles for all raining pixels are computed separately for February and August in Figure 4a,c, and conditional reflectivity profiles (average of all profiles with PR reflectivity at each altitude) are computed in Figure 4b,d. These two months correspond to extremes of the seasonal cycle for deep convection in the region. In February, the tallest radar profiles in the region reach their southernmost extent directly over the shipping lane. As the year progresses, intense convection migrates northward until it reaches its northernmost extent in August. This leaves the shipping lane at a local minimum in the PR profile data. The 0.5 – 1.0 dBZ difference at high altitudes in Thornton et al. (2017) may be due to the shipping lane being co-located with the extremes of the seasonal cycle, unrelated to the shipping traffic through the region.

Moreover, the variability in the mean reflectivity profiles in Figure 4 demonstrates why relying on the PR reflectivity profile data is problematic: biases from individual large thunderstorms. Figure 5 uses the RPF pixel counts over the domain in Figure 2 to quantify the severity of this problem. For all storm types in the Bay of Bengal, 35% of RPFs contain a single raining pixel and would produce equivalent results to the PR profile approach. However, that fraction falls to 27% for features that extend to the altitudes where Thornton et al. (2017) noted enhanced reflectivities over the shipping lane (> 7 km), and to only a few percent for thunderstorms. Meanwhile, the median RPF raining PR pixel counts in the latter two categories are around 10 and 100, respectively, and the largest RPFs in the region can individually encompass 10,000 raining pixels.

Our TRMM and WWLLN analyses support the idea that the lightning enhancement over the Bay of Bengal shipping lane results from shipping traffic facilitating lightning initiation. However, the enhancement does not appear to be accompanied by a clear modification to the intensity or microphysical properties of storms over the shipping lane that is expected in the aerosol hypothesis put forward by Thornton et al. (2017).

3.2 Lightning Enhancements Near Maritime Traffic from Direct Ship Interactions

Thornton et al. (2017) argued that aerosols, rather than direct lightning interactions with ships, are responsible for the enhanced lightning activity over shipping lanes because the width of the WWLLN signature in the Bay of Bengal was greater than the width of the shipping lane in the EDGAR data. Lightning strikes on ships must occur at the current location of the ship. At the same time, there is no such restriction on lightning enhancements from aerosols. The ship exhaust will be advected downwind where it may modify convective processes at variable distances and directions from the emissions source. As the WWLLN thunderstorm areas hardly propagate in most cases (Figure 2c), we would expect to find a broad peak that is still centered on the shipping lane under this explanation, consistent with the results from Thornton et al. (2017).

There are two problems with this argument, however. The first is that the increased width of the WWLLN signature relative to the EDGAR emissions data does not rule out ship interactions as being responsible for the factor-of-two peak WWLLN enhancement over the shipping lane. Aerosol effects and lightning strikes on / around ships can both simultaneously contribute to the observed enhancement, and their relative contributions can vary spatially. For example, the weaker enhancements outside of the shipping lane (i.e, beyond the 10% lines in Figure 2) may be primarily due to aerosol effects. Yet, this leads to the second problem: the EDGAR emissions data show that maritime traffic is not zero in the WWLLN enhancement region outside of the primary shipping lane. Lightning enhancements from ship strikes may not be a linear function of the number density of shipping traffic, and if the mouth of the Bay of Bengal is naturally prone to creating borderline ESCs, then the smaller number of vessels outside of the shipping lane could still contribute to the broader peak.

To further explore these possibilities, this section will move from large-scale EDGAR correlations to individual matches between AIS transponder events and WWLLN strokes. However, we cannot distinguish between lightning strikes on ships and strokes that attach to seawater close to a ship using WWLLN due to its kilometer-scale location accuracy. We consider a pronounced narrow peak at the current ship location to be evidence of ship interactions, without differentiating between these possibilities. Future work will use a lightning detection network with a finer location accuracy to separate close lightning strikes on seawater from lightning strikes on ships.

We identify these close lightning events as a subset of the WWLLN strokes (Figure 1b) that are matched to any of the AIS events from the NOAA dataset (Figure 6a), as described in Section 2. Generous matching criteria of 0.5 degrees and 10 minutes are used to generate the distribution of WWLLN events in the vicinity of shipping traffic in Figure 6b. Then, close WWLLN matches are designated as any matched event that occurs within the nominal WWLLN location accuracy of an oceangoing vessel. Note that our samples of all WWLLN matches and close WWLLN matches will be subject to the sampling biases in the NOAA AIS data that are evident in Figure 6a. The only filtering that we apply is to remove inland AIS events and to restrict the northern extent of the plot due to a lack of Arctic lightning events. The hard boundaries at 60 W and the equator, and the inconsistent sampling west of the international date line are caused by limitations in the NOAA AIS data. Most of the matched WWLLN strokes to AIS events in Figure 6b occur along the southern and eastern coasts of the continental United States – extending further offshore than the maximum in AIS event density from Figure 6a – but there are also large clusters of matched events surrounding Guam, Hawaii, the California coast, and Puerto Rico, as well as collections of infrequent events in open ocean regions.

For all of these matches, we compute the difference in position between the WWLLN stroke and the AIS event. The latitude and longitude displacements of WWLLN strokes relative to ship locations are shown in Figure 7. The plan view in Figure 7b depicts how often lightning within a 0.5 degree radius strikes each point surrounding the ship in geographic coordinates. The distribution is flat at large distances, indicating no location preference when lightning occurs far from the ship. This can also be noted in the longitude and latitude cross sections through the center of the distribution in Figure 7a and c.

Multiple types of enhanced WWLLN activity can be noted closer to the ship in Figure 7. The most prominent enhancement is the narrow peak centered on the vessel position at the center of the distribution. We attribute this peak to direct ship interactions where the presence of the vessel increases the likelihood of lightning strikes. Aerosol effects would be located beyond this narrow peak where two distinct types of enhancement are evident. The first is a broad low-amplitude peak surrounding the ship, which may also be due to variable WWLLN location accuracy. The second manifests as linear paths extending through the center of the image, preferentially at certain angles. The linear enhancements trace out the paths of the most common shipping lanes in the NOAA AIS data. We use the ship heading information recorded in the AIS data to compute the frequency of matched WWLLN events relative to along track and cross track distances in Figure 8a. The peak of the distribution remains at the ship location, but rotating the coordinate system relative to the ship's course elongates the enhancement signature in the along track direction, as the linear features in Figure 7b become superimposed on the same axis. The along track event totals in Figure 8b show a far more gradual decrease over the 50 km range depicted in the figure than the cross sections from Figure 7.

This enhancement following the shipping lane along distances 25 km or greater from the closest vessel might appear to provide evidence for an aerosol effect similar to the ship track clouds whose widths are also ~25 km. However, if convection were initiating preferentially over the ship track due to the shipping exhaust, then we would not expect the enhanced signal to be confined to just ~2 km in the cross-track direction. If it were, then aerosol effects could not explain the broader WWLLN signature over the Bay of Bengal. We might also expect to find a slight enhancement behind the ship compared to out ahead of the ship, yet the lightning totals in Figure 8b are symmetrical about the ship position. There is an alternate explanation for why lightning enhancements might occur only along the ship track from the relevant maritime law: exemptions to the required use of AIS transponders, particularly from domestic shipping. Domestic-bound vessels are not required to have operational AIS transponders and might not be included in our catalog of AIS events. Moreover, vessels that are not required to maintain an active AIS transponder over the duration of their voyages may choose to only activate it intermittently. These vessels would still be susceptible to being struck by lightning, resulting in increased WWLLN detections along the common shipping routes, but the signal would not be confined to 0 km in the along track direction due to the incomplete AIS data.

This ambiguous enhancement is not present in the cross-track direction, allowing us to compare the relative magnitudes of the narrow peak from direct ship interactions with the broad enhancements that might result from aerosol effects. Figure 9 shows a cross-track slice through

Figure 8 within 2 km of the ship position in the along-track direction. Since the narrow peak at the ship position in Figure 9 has a greater amplitude relative to the surrounding oceans than the along-track integration in Figure 8b, we show the distribution on a logarithmic scale normalized to the maximum amplitude. A Cumulative Distribution Function (CDF) across the ship track is also overlaid in black.

The lightning distribution is dominated by the central peak at the ship location. When lightning occurs in a convective-scale (10-20 km) region surrounding shipping traffic, the likelihood of the stroke occurring at the ship location is enhanced by ~50x compared to the edge of the domain. 38% (31%) of all strokes that occur over the 50 km cross section are located within 2 km (1 km) of the ship. Outside of this narrow peak, the amplitude of the enhancement decreases slowly with distance due to a combination of WWLLN location errors and, potentially, aerosol enhancements. Unlike the along-track distribution, the cross-track distribution is not symmetric. 28% of strokes occur >2 km to the left of the ship's course, while 34% occur >2 km to the right of the ship. This could be caused by land / sea effects or evidence of a systematic WWLLN offset, as seen previously (Abarca et al., 2010) – though such an offset would have to be situational to maintain the stroke density peak at the center of the ship track. However, it could also be evidence of preferential wind directions causing increased aerosol enhancements in certain directions over others.

Even if we assume that all WWLLN enhancements >2 km from the ship location can solely be attributed to aerosol effects, the amplitude of the enhancement (the measured quantity in Thornton et al., 2017) is only on the order of a few percent compared to the edge of the domain, and at least an order of magnitude smaller than the narrow peak from direct ship interactions. The role of aerosols in the complex series of atmospheric processes that leads to lightning initiation is both subtle and nuanced, and evidence of aerosol effects must compete with strong natural and manmade trends in the data. More work is needed to separate the aerosol signal in the lightning data from other factors.

3.3 Frequencies of Lightning Interactions with Ships in the NOAA AIS Dataset

Matching WWLLN strokes with AIS transponder events from the NOAA catalog allows us to document the frequency of close ship interactions with lightning by vessel type, and even for individual vessels. In this section, we use the vessel information fields in the AIS data to take a detailed look at these close WWLLN matches to AIS events that are either direct strikes on the ship or at a close enough range to pose a particular hazard.

Unfortunately, the AIS data does not include information about vessel heights above the sea surface, which would be the key parameter for understanding lightning interactions. Instead, we will use the vessel dimensions as a rough proxy for vessel height. Note that the AIS catalog includes vessels such as oil rigs whose "length" and "width" values might not be intuitive. Figure 10 compares the reported vessel lengths and widths in the overall AIS dataset (red) with only those AIS events that are closely matched with WWLLN (blue). The left panels (Figure 10a and c) include all AIS transponder events while each vessel is at sea, weighting the distributions according to the amount of time the vessels in each bin spends in active service. For each of these bins, the frequency of close WWLLN matches is roughly four orders of magnitude lower than the total number of AIS events. In total, direct vessel lightning exposure rates are around

0.004%. However, these rates fluctuate according to vessel type, which can be noted in the ship size data. The CDFs in Figure 10a and c indicate that mid-to-large vessels account for a greater share of the close WWLLN matches than their overall proportion of the AIS data would suggest.

The right panels in Figure 10 (Figure 10b and d) compare the frequencies of all AIS events from unique vessel Marine Mobile Service Identities (MMSIs) (red) with those that have had a close WWLLN match (blue). While direct lightning interactions account for a small percentage of all AIS events, the frequencies of ships that have potentially been struck ranges from a few percent to over 10%, depending on the length and width of the vessel. As before, mid-to-large ships are more likely to have a close WWLLN match than smaller vessels.

The likelihood of a ship having a direct lightning interaction should depend on both its construction and the amount of time it spends around active thunderstorms. Even large / tall vessels operating off the coast of California are unlikely to be struck by lightning due to the limited number of strokes that occur in the area. When vessels must operate in storm-prone regions in the Gulf of Mexico or along the Gulf Stream, their increased exposure to lightning raises the likelihood of being struck – especially for commercial vessels that are financially motivated to sail through oceanic thunderstorms to reach their destinations.

We would thus expect the frequencies of close WWLLN events in Figure 10 to differ according to the vessel categories listed in the AIS data. We have combined the multitude of similar categories into 8 distinct sectors: fishing, towing (including port facilities), sailing, pleasure craft, passenger vessels, cargo vessels, tanker vessels, and none / other (including AIS entries without the vessel category specified). Pie charts of the vessels in these categories are shown in Figure 11. Figure 11a depicts the composition of all maritime traffic in the NOAA dataset. The most common categories are pleasure craft (19,921 vessels), cargo ships (10,206 vessels), and sailing ships (7,483 vessels). Together, these three categories comprise 68% of all traffic.

However, the frequencies of vessels that have had a close lightning encounter in each category differ from the fleet composition in Figure 11a. Figure 11b counts the number of vessels in each category with at least one close WWLLN stroke. In total, 14,184 of the 55,327 vessels from Figure 11a -25% of the total - had a close lightning encounter in the 1/1/2019 – 12/31/2021 period considered in this study. Despite accounting for just 19% of all maritime traffic, 26% of the close WWLLN strokes occurred with cargo ships, making it the top ranked category for lightning interactions. 3,658 of the 10,206 cargo ships in the NOAA AIS catalog have had a close WWLLN stroke – 36% of the cargo fleet. Pleasure craft are the second most common category for lightning interactions, accounting for 19% of the total, though the fraction of all vessels with a close WWLLN match is only 13%. Tanker ships, meanwhile, accounted for a further 18% of close WWLLN matches. 2,558 of the total 4,079 tanker ships in the AIS dataset had a lightning encounter, representing 62% of the fleet. Sailing ships, by contrast, had the lowest rate of lightning interactions of our 8 categories, with only 9% having a close WWLLN match over the 3-year period.

Individual vessels have also had multiple lightning interactions. The total number of close WWLLN strokes for all vessels in each category are computed in Figure 11c. Allowing repetition weights the distribution from Figure 11b to account for the varying amount of time the ships in each category spend under lightning hazards. The tanker and cargo ship fractions are nearly the same in this new weighting, but the contribution from passenger ships is nearly doubled, while the pleasure craft and sailing ship contributions are reduced by nearly half. This is consistent with expectations that the latter two categories have the greatest flexibility to avoid storms. There are also increased contributions from fishing vessels, as well as the none / other category, which includes offshore platforms.

The ships that have direct lightning encounters tend to have multiple close WWLLN events. This can include multiple potential strikes during a single voyage through a thunderstorm, or due to static routes that frequently take the vessel through lightning-prone regions. Figure 12 computes the frequency of close WWLLN matches for each unique vessel MMSI that has had a close lightning encounter over the 3-year period. Only 1-in-5 of these vessels had just one close WWLLN match. The median is ~5 strokes in 3 years, and one-third of vessels exposed to lightning had greater than 10 close WWLLN matches in this time. The tip of this distribution includes vessels with dozens or even hundreds of close lightning encounters. We list the top 25 of these vessels in Table 1. Nearly half of the vessels in Table 1 are 30-60 m offshore supply boats / crew boats - vessels that transport crew and supplies to offshore installations. The vessel with the most lightning encounters was the Shelby Courtney, which operates around Gulf Coast Louisiana and was within 2 km of 449 WWLLN strokes during the 3-year period. The second vessel by stroke count is the 187 m cargo ship Bahama Spirit with 444 close lightning encounters. Cargo and tanker ships account for 5 of the top 25 vessels in Table 1, while there are also 3 tugs, 1 dredger, and 1 fishing boat. There are no pleasure craft or sailing ships in Table 1, but the top 25 ships by close lightning encounters do include 3 cruise ships: the Disney Dream with 413 strokes, the Disney Fantasy with 290 strokes, and the Carnival Pride with 270 strokes. The variety of vessel sizes and categories in Table 1 suggests that the amount of time spent sailing in lightning-prone regions is the primary driver of close lightning encounters. All of these vessels spent hundreds of days at sea over the 3-year period, and the hundreds of WWLLN matches only account for < 0.3% of the AIS data generated by each of these vessels.

The fractions of WWLLN-matched AIS events can be considerably greater, however. We rank the vessels with frequent lightning encounters (≥ 5 strokes in 3 years) by the percent of AIS events that have close WWLLN matches, and list the top 25 vessels in Table 2. These vessels left port on 30-or-fewer days over the 3 year period, but these voyages preferentially occurred during hazardous conditions for lightning interactions – resulting in between 1.8% and 45.4% of all AIS events generated by each vessel occurring in close proximity to a WWLLN stroke. The top vessel by WWLLN-matched AIS fraction is clearly an outlier, though it is unclear why 241 of the 531 total AIS events from the Karon Louise recorded over a period of 8 days matched a WWLLN stroke. As the vessel is a pleasure craft and probably not required to keep its AIS transponder active, it is likely that the captain elected to turn it on when they encountered hazardous conditions at sea. In total, 9 of the top 25 vessels by lightning-matched AIS event fractions were pleasure craft, while 7 were cargo ships, 4 were sailing ships, 3 were government vessels, and 2 were unknown. Actual stroke rates ranged from our arbitrary minimum of 5 to the Karon Louise's 241 strokes in 3 years. In contrast to the top pleasure crafts' ratios exceeding 10%, the top cargo ships fall in the 1-4% range and are comprised of a few hundred to a few thousand AIS events. This order of magnitude increase from the top stroke count cases in Table

1 is probably a reasonable estimate of peak AIS WWLLN-matched fractions without manmade sampling biases.

4 Conclusions

This study examines lightning interactions with maritime traffic. Thornton et al. (2017) noted an enhancement in lightning activity over two shipping lanes, and attributed this increase in lightning frequency to the aerosols in ship exhaust modifying convective processes responsible for lightning generation, resulting in stronger storms over the shipping lanes compared to nearby clean ocean regions. They discounted direct lightning strikes on ships as the cause of this enhancement because the signature in the lightning data appeared to be wider than the shipping lane. Their primary evidence for storm modifications came from a slight (~0.5-1 dBZ) enhancement in TRMM PR reflectivity profiles at high altitudes over the shipping lane.

Our analyses indicate that the enhanced lightning signal identified by Thornton et al. (2017) over the Bay of Bengal is not accompanied by a clear variation in storm properties over the shipping lanes. Thunderstorm stroke rates reported by WWLLN and storm-level TRMM proxies for convective intensity are not notably different between the shipping lane and the surrounding clean ocean regions, aside from the large-scale natural variations in the region (i.e., terrain effects, the Indian monsoon, etc.). The reflectivity enhancement discussed by Thornton et al. (2017) exists only in the radar profile data, where individual storms are able to contribute multiple profiles to the sample – causing the largest / strongest storms to have an outsized impact on the statistics. We have not identified a clear sign of aerosol effects over the shipping lane in the microphysical parameters measured by TRMM.

In contrast to the prior work, we do find evidence of a strong signature of lightning enhancement from direct lightning interactions with oceangoing vessels. When lightning occurs within a convective-scale region surrounding a ship, the stroke is much more likely to occur at the location of the ship than anywhere else in the domain. Due to the limited location accuracy of WWLLN, we cannot verify whether lightning struck the ship or if it attached to seawater near the ship's location. However, the 1-2 orders of magnitude enhancement to WWLLN stroke frequencies at the ship location makes it clear that the presence of the vessel directly influenced the stroke. Elevated lightning rates at larger distances are either the result of poor WWLLN geolocation solutions or aerosol effects. If we assume that all of the spread comes from the latter, we can estimate the maximum magnitude of aerosol enhancements at ~6% of the overall lightning enhancement in the vicinity of the ship.

The frequency of close lightning encounters depends on the amount of time each vessel spends traversing lightning-prone regions, ship construction, and vessel category. Ships that have the greatest exposure to lightning tend to be moderate-to-large commercial vessels that may be motivated to sail through stormy conditions rather than avoid foul weather. Thus, cargo ships, tanker ships, and passenger ships have greater incidences of close WWLLN strikes than pleasure craft or sailing vessels. The ships with the most close lightning encounters are offshore supply boats, cargo / tanker ships, tug / towing / dredging vessels, fishing boats, and cruise ships – with certain individual vessels having up to 270-449 close lightning strokes over a 3-year period. Meanwhile, the vessels that have the greatest fractions of AIS events closely matching WWLLN strokes are primarily pleasure craft, cargo ships, sailing ships, and government vessels. These ships are either infrequently used or are not required to have an active AIS transponder while under way. Pleasure craft, in particular, may be biased if they only turn on their transponders when they encounter trouble at sea (i.e., a thunderstorm).

These results demonstrate that the connections between the natural environment and human activities are rarely simple or clear-cut. We do not know to what extent the increased aerosol emissions from shipping traffic are modifying deep convection across the world's oceans. In the search for this answer, we should not overlook alternate explanations for the signals that we find in our data. Nor should we ignore the fact that only two of the world's shipping lanes show clear evidence of an anthropogenic lightning enhancement. Based on all available evidence, we propose that these signals only arise because the Bay of Bengal and the South China Sea frequency produce ESCs that nearly become thunderstorms, and that the presence of shipping traffic facilitates this transition. We do not see enhancements in other regions because the environment is either not conducive to electrification, or the region already contains active thunderstorms that dominate the lightning signal. More work is needed to understand these complex Earth system interactions, and the role of shipping traffic in atmospheric electricity.

Acknowledgments

Los Alamos National Laboratory is operated by Triad National Security, LLC, under contract number 89233218CNA000001.

Open Research

The processed data used in this study are available at the Harvard Dataverse via DOI: 10.7910/DVN/HMADPN (Peterson, 2023). WWLLN stroke data may be acquired by requesting the data from the University of Washington. The NOAA AIS dataset may be accessed via MarineCadastre.gov (NOAA, 2022), a data infrastructure collaboration between NOAA and the Bureau of Ocean Energy Management.

References

Abarca, S. F., Corbosiero, K. L., & Galarneau Jr, T. J. (2010). An evaluation of the worldwide lightning location network (WWLLN) using the national lightning detection network (NLDN) as ground truth. *Journal of Geophysical Research: Atmospheres*, *115*(D18).

Arcanjo, M., Montanyà, J., Urbani, M., Lorenzo, V., & Pineda, N. (2021). Observations of corona point discharges from grounded rods under thunderstorms. *Atmospheric Research*, *247*, 105238.

Aleksandrov, N. L., Bazelyan, E. M., Carpenter Jr, R. B., Drabkin, M. M., & Raizer, Y. P. (2001). The effect of coronae on leader initiation and development under thunderstorm conditions and in long air gaps. *Journal of Physics D: Applied Physics*, *34*(22), 3256.

Aleksandrov, N. L., Bazelyan, E. M., Drabkin, M. M., Carpenter, R. B., & Raizer, Y. P. (2002). Corona discharge at the tip of a tall object in the electric field of a thundercloud. *Plasma Physics Reports*, *28*(11), 953-964.

Aleksandrov, N. L., Bazelyan, E. M., & Raizer, Y. P. (2005). The effect of a corona discharge on a lightning attachment. *Plasma physics reports*, *31*(1), 75-91.

Bazelyan, E. M., Raizer, Y. P., & Aleksandrov, N. L. (2008). Corona initiated from grounded objects under thunderstorm conditions and its influence on lightning attachment. *Plasma Sources Science and Technology*, *17*(2), 024015.

Bernstein, T., & Reynolds, T. S. (1978). Protecting the Royal Navy from Lightning-William Snow Harris and His Struggle with the British Admiralty for Fixed Lightning Conductors. *IEEE Transactions on Education*, *21*(1), 7-14.

Capaldo, K., Corbett, J. J., Kasibhatla, P., Fischbeck, P., & Pandis, S. N. (1999). Effects of ship emissions on sulphur cycling and radiative climate forcing over the ocean. *Nature*, *400*(6746), 743-746.

Carey, L. D., Murphy, M. J., McCormick, T. L., & Demetriades, N. W. (2005). Lightning location relative to storm structure in a leading-line, trailing-stratiform mesoscale convective system. *Journal of Geophysical Research: Atmospheres*, *110*(D3).

Christian, H. J. (1994). Algorithm theoretical basis document (ATBD) for the Lightning Imaging Sensor (LIS). *http://thunder. msfc. nasa. gov/bookshelf/pubs/atbd/*.

Crippa, M., Guizzardi, D., Muntean, M., Schaaf, E., MONFORTI-FERRARIO, F., BANJA, M., ... & SOLAZZO, E. (2019). EDGAR v6. 1 global air pollutant emissions.

Cockbain, T. G. E. (1945). Manifestations of St. Elmo's Fire in a Tropical Storm. *The Aeronautical Journal*, *49*(413), 289-290.

Conover, J. H. (1966). Anomalous cloud lines. *Journal of Atmospheric Sciences*, *23*(6), 778-785.

Cummins, K. L., & Murphy, M. J. (2009). An overview of lightning locating systems: History, techniques, and data uses, with an in-depth look at the US NLDN. *IEEE transactions on electromagnetic compatibility*, *51*(3), 499-518.

Dallinger, W. H. (1889). ST. ELMO'S FIRE, AND THE OBSERVATORY ON BEN NEVIS. *The Wesleyan-Methodist magazine*, 779-780.

Forti, N., d'Afflisio, E., Braca, P., Millefiori, L. M., Willett, P., & Carniel, S. (2021). Maritime anomaly detection in a real-world scenario: Ever Given grounding in the Suez Canal. *IEEE Transactions on Intelligent Transportation Systems*, *23*(8), 13904-13910.

Han, Q., Rossow, W. B., Chou, J., & Welch, R. M. (1998). Global variation of column droplet concentration in low-level clouds. *Geophysical Research Letters*, *25*(9), 1419-1422.

Hutchins, M. L., Holzworth, R. H., Brundell, J. B., & Rodger, C. J. (2012). Relative detection efficiency of the world wide lightning location network. *Radio Science*, *47*(06), 1-9.

International Maritime Organization. (2019). AIS transponders. Retrieved December 30, 2022, from https://www.imo.org/en/OurWork/Safety/Pages/AIS.aspx

Jacobson, A. R., Holzworth, R., Harlin, J., Dowden, R., & Lay, E. (2006). Performance assessment of the world wide lightning location network (WWLLN), using the Los Alamos sferic array (LASA) as ground truth. *Journal of Atmospheric and Oceanic Technology*, *23*(8), 1082-1092.

Jalkanen, J. P., Johansson, L., Kukkonen, J., Brink, A., Kalli, J., & Stipa, T. (2012). Extension of an assessment model of ship traffic exhaust emissions for particulate matter and carbon monoxide. *Atmospheric Chemistry and Physics*, *12*(5), 2641-2659.

Johansson, L., Jalkanen, J. P., & Kukkonen, J. (2017). Global assessment of shipping emissions in 2015 on a high spatial and temporal resolution. *Atmospheric Environment*, *167*, 403-415.

Kozu, T., Kawanishi, T., Kuroiwa, H., Kojima, M., Oikawa, K., Kumagai, H., ... & Nishikawa, K. (2001). Development of precipitation radar onboard the Tropical Rainfall Measuring Mission (TRMM) satellite. *IEEE transactions on geoscience and remote sensing*, *39*(1), 102-116.

Kummerow, C., Barnes, W., Kozu, T., Shiue, J., & Simpson, J. (1998). The tropical rainfall measuring mission (TRMM) sensor package. *Journal of atmospheric and oceanic technology*, *15*(3), 809-817.

Lay, E. H., Holzworth, R. H., Rodger, C. J., Thomas, J. N., Pinto Jr, O., & Dowden, R. L. (2004). WWLL global lightning detection system: Regional validation study in Brazil. *Geophysical Research Letters*, *31*(3).

Lightning. (1840). *The Nautical Magazine and Naval Chronicle*. 387-387.

Liu, C., Zipser, E. J., Cecil, D. J., Nesbitt, S. W., & Sherwood, S. (2008). A cloud and precipitation feature database from nine years of TRMM observations. *Journal of Applied Meteorology and Climatology*, *47*(10), 2712-2728.

Lundquist, S. (1985). On the discharge of static electricity: Some historic notes with comments and remarks. *Journal of Electrostatics*, *16*(2-3), 221-230.

Mach, D. M., Christian, H. J., Blakeslee, R. J., Boccippio, D. J., Goodman, S. J., & Boeck, W. L. (2007). Performance assessment of the optical transient detector and lightning imaging sensor. *Journal of Geophysical Research: Atmospheres*, *112*(D9).

Mach, D. M., Blakeslee, R. J., & Bateman, M. G. (2011). Global electric circuit implications of combined aircraft storm electric current measurements and satellite-based diurnal lightning statistics. *Journal of Geophysical Research: Atmospheres*, *116*(D5).

Montanyà, J., Van Der Velde, O., & Williams, E. R. (2014). Lightning discharges produced by wind turbines. *Journal of Geophysical Research: Atmospheres*, *119*(3), 1455-1462.

NOAA. (2022). *Vessel Traffic Data*. MarineCadastre.gov | Vessel Traffic Data. Retrieved December 30, 2022, from https://marinecadastre.gov/ais/

O'Dowd, C. D., Smith, M. H., Consterdine, I. E., & Lowe, J. A. (1997). Marine aerosol, sea-salt, and the marine sulphur cycle: A short review. *Atmospheric Environment*, *31*(1), 73-80.

Olivier, J. G. J., Bouwman, A. F., Van der Maas, C. W. M., & Berdowski, J. J. M. (1994). Emission database for global atmospheric research (EDGAR). *Environmental Monitoring and Assessment*, *31*(1), 93-106.

Peterson, M. (2023) Ship Lightning Interactions Data, https://doi.org/10.7910/DVN/HMADPN, Harvard Dataverse, V2

Plinius, Gaius II (77). Or the stars which are named Castor and Pollux. In Historia Naturalis (Vol. 2, Ch. 37).

Priestley, J. (1775). *“The” History and Present State of Electricity: With Original Experiments*. C. Bathurst and T. Lowndes, in Fleet-Street, J. Rivington and J. Johnson, in St. Paul's Church-Yard, S. Crowder, G. Robinson, and R. Baldwin, in Paternoster Row, T. Becket and T. Cadell, in the Strand.

Rodger, C. J., Werner, S., Brundell, J. B., Lay, E. H., Thomson, N. R., Holzworth, R. H., & Dowden, R. L. (2006, December). Detection efficiency of the VLF World-Wide Lightning Location Network (WWLLN): initial case study. In *Annales Geophysicae* (Vol. 24, No. 12, pp. 3197-3214). Copernicus GmbH.

Ship destroyed by lightning. (1846). *Scientific American.* 106-106.

Schreier, M., Mannstein, H., Eyring, V., & Bovensmann, H. (2007). Global ship track distribution and radiative forcing from 1 year of AATSR data. *Geophysical Research Letters*, *34*(17).

Schumann, C., Saba, M. M., Warner, T. A., Ferro, M. A., Helsdon, J. H., Thomas, R., & Orville, R. E. (2019). On the triggering mechanisms of upward lightning. *Scientific Reports*, *9*(1), 1-9.

Thomas, R. J., Krehbiel, P. R., Rison, W., Hunyady, S. J., Winn, W. P., Hamlin, T., & Harlin, J. (2004). Accuracy of the lightning mapping array. *Journal of Geophysical Research: Atmospheres*, *109*(D14).

Thornton, J. A., Virts, K. S., Holzworth, R. H., & Mitchell, T. P. (2017). Lightning enhancement over major oceanic shipping lanes. *Geophysical Research Letters*, *44*(17), 9102-9111.

Wang, D., & Takagi, N. (2012). Characteristics of winter lightning that occurred on a windmill and its lightning protection tower in Japan. *IEEJ Transactions on Power and Energy*, *132*(6), 568-572.

Warner, T. A., Lang, T. J., & Lyons, W. A. (2014). Synoptic scale outbreak of self-initiated upward lightning (SIUL) from tall structures during the central US blizzard of 1–2 February 2011. *Journal of Geophysical Research: Atmospheres*, *119*(15), 9530-9548.

Wescott, E. M., Sentman, D. D., Heavner, M. J., Hallinan, T. J., Hampton, D. L., & Osborne, D. L. (1996). The optical spectrum of aircraft St. Elmo's fire. *Geophysical research letters*, *23*(25), 3687-3690.

Whipple, F. J. W. and F. J. Scrase (1936). Point-discharge in the electric field of the Earth. *Geophys. Mem. VII*, *68*, 1-20.

Wu, T., Wang, D., Rison, W., Thomas, R. J., Edens, H. E., Takagi, N., & Krehbiel, P. R. (2017). Corona discharges from a windmill and its lightning protection tower in winter thunderstorms. *Journal of Geophysical Research: Atmospheres*, *122*(9), 4849-4865.

Table 1. The top 25 vessels by close WWLLN stroke counts between 1/1/2019 and 12/31/2021

Close WWLLN Strokes	Total AIS Events	Close WWLLN Fraction (%)	Days with AIS Events	Vessel Length (m)	Vessel Width (m)	Vessel Name	Vessel Category
449	175,810	0.26	500	34	7	Shelby Courtney	Offshore Supply Boat
444	422,063	0.11	897	187	32	Bahama Spirit	Cargo Ship
425	442,975	0.10	884	52	9	Grey Cup	Offshore Supply Boat
413	278,612	0.15	841	339	40	Disney Dream	Cruise Ship
381	441,490	0.09	765	50	9	Gol Intruder	Offshore Supply Boat
374	254,498	0.15	534	42	13	Abundance	Tug
373	213,868	0.17	431	-----	-----	Cape Hatteras	Towing Vessel
357	852,191	0.04	1056	41	8	Diamond Mine	Offshore Supply Boat
357	466,769	0.08	797	94	15	Columbia	Dredger
336	119,186	0.28	650	58	9	Fast Leopard	Offshore Supply Boat
327	66,693	0.49	189	182	40	Donna	Tanker Ship
314	389,927	0.08	1019	45	10	Dustin Danos	Offshore Supply Boat
312	141,336	0.22	373	249	43	Chrysalis	Tanker Ship
301	334,931	0.09	719	90	17	Tropic Lure	Cargo Ship
300	542,145	0.06	991	36	7	Eveready	Offshore Supply Boat
294	457,764	0.06	954	49	13	Odyssea Darwin	Offshore Supply Boat
292	683,528	0.04	790	48	9	Sea Angel	Offshore Supply Boat
291	467,655	0.06	651	24	7	St. Peter	Fishing Boat
290	259,229	0.11	719	339	40	Disney Fantasy	Cruise Ship
289	227,443	0.13	576	224	32	Camila B	Tanker Ship
284	368,639	0.08	643	36	10	Scott Turecamo	Tug
283	437,353	0.06	693	58	12	Odyssea Defender	Offshore Supply Boat
282	580,801	0.05	986	44	8	Anna M	Offshore Supply Boat

795 **Table 2.** The top 25 vessels by close WWLLN stroke fractions of all AIS events between
796 1/1/2019 and 12/31/2021
797

Close WWLLN Strokes	Total AIS Events	Close WWLLN Fraction (%)	Days with AIS Events	Vessel Length (m)	Vessel Width (m)	Vessel Name	Vessel Category
241	530	45.47	8	17	4	Karon Louise	Pleasure Craft
28	176	15.91	7	12	7	-----	-----
5	46	10.87	2	21	6	Holiday	Local Vessel
70	648	10.80	13	11	4	Jully Roger IX	Pleasure Craft
25	291	8.59	17	276	32	USNS Yano	Government
22	338	6.51	9	54	12	Lake Guardian	Government
20	335	5.97	7	14	5	Abyss	Pleasure Craft
21	441	4.76	3	19	5	Rosa del Mar	Sailing Ship
45	1169	3.85	3	182	27	Ippokratis	Cargo Ship
59	1597	3.69	15	13	5	Barefoot Jones	Pleasure Craft
13	418	3.11	16	-----	-----	Nighthawk	Government
7	236	2.97	8	12	4	Sweet Tides	Sailing Ship
38	1342	2.83	13	13	22	Olivia	Pleasure Craft
10	420	2.38	8	14	4	Island Time	Pleasure Craft
12	512	2.34	1	225	32	Magic Phoenix	Cargo Ship
64	2829	2.26	10	180	32	Isabella M	Cargo Ship
5	228	2.19	9	13	3	Wings	Sailing Ship
48	2230	2.15	10	189	28	Podlasie	Cargo Ship
54	2541	2.13	9	288	45	Ocean Caesar	Cargo Ship
104	5010	2.08	10	189	28	Pomorze	Cargo Ship
232	11712	1.98	30	35	7	Mimi	Pleasure Craft
48	2523	1.90	9	224	32	Asia Graeca	Cargo Ship
10	527	1.90	5	10	4	Catch This	Pleasure Craft

798

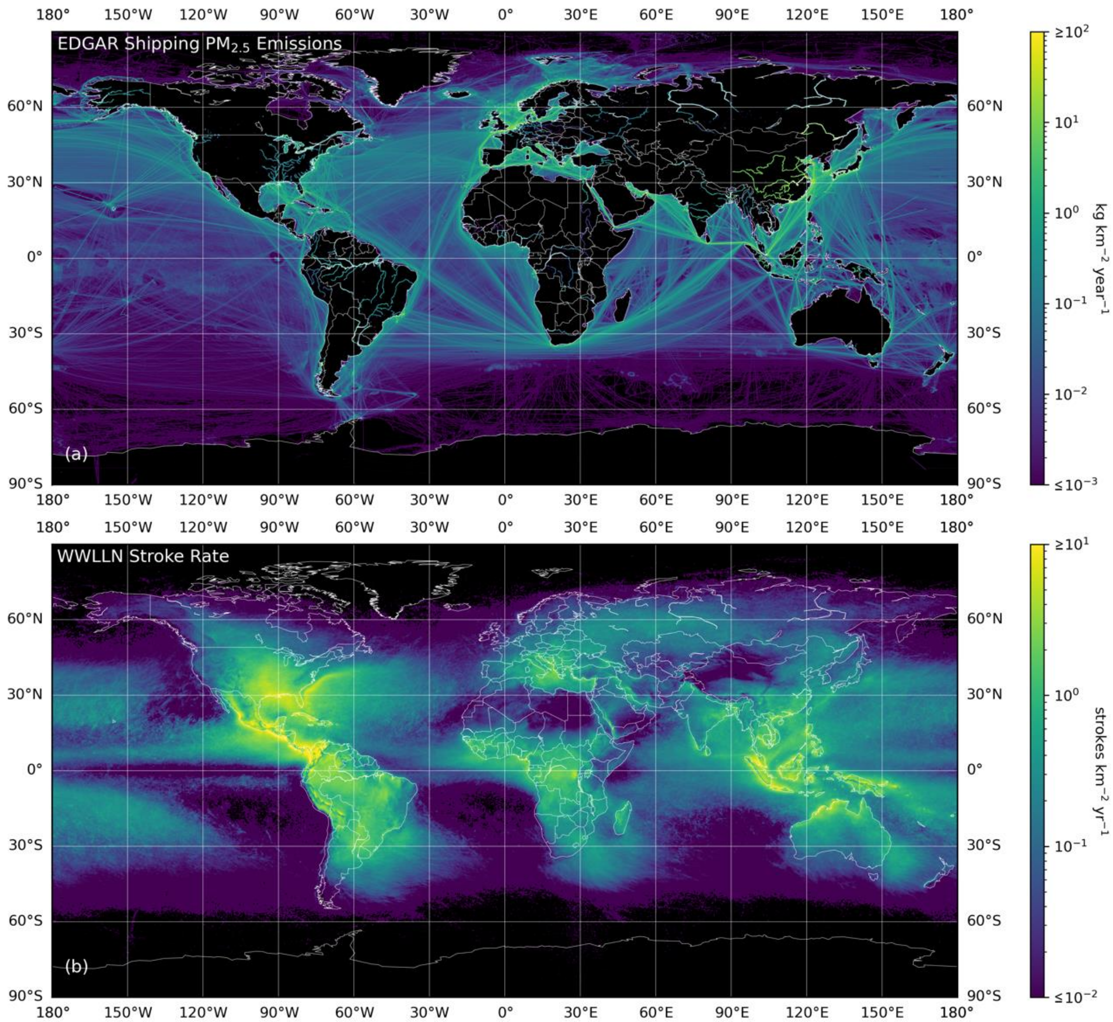

Figure 1. Global distributions of the annual average (a) EDGAR $PM_{2.5}$ shipping emissions and (b) WWLLN stroke rates. Note that the color bar ranges have been restricted to highlight activity over the sea lanes.

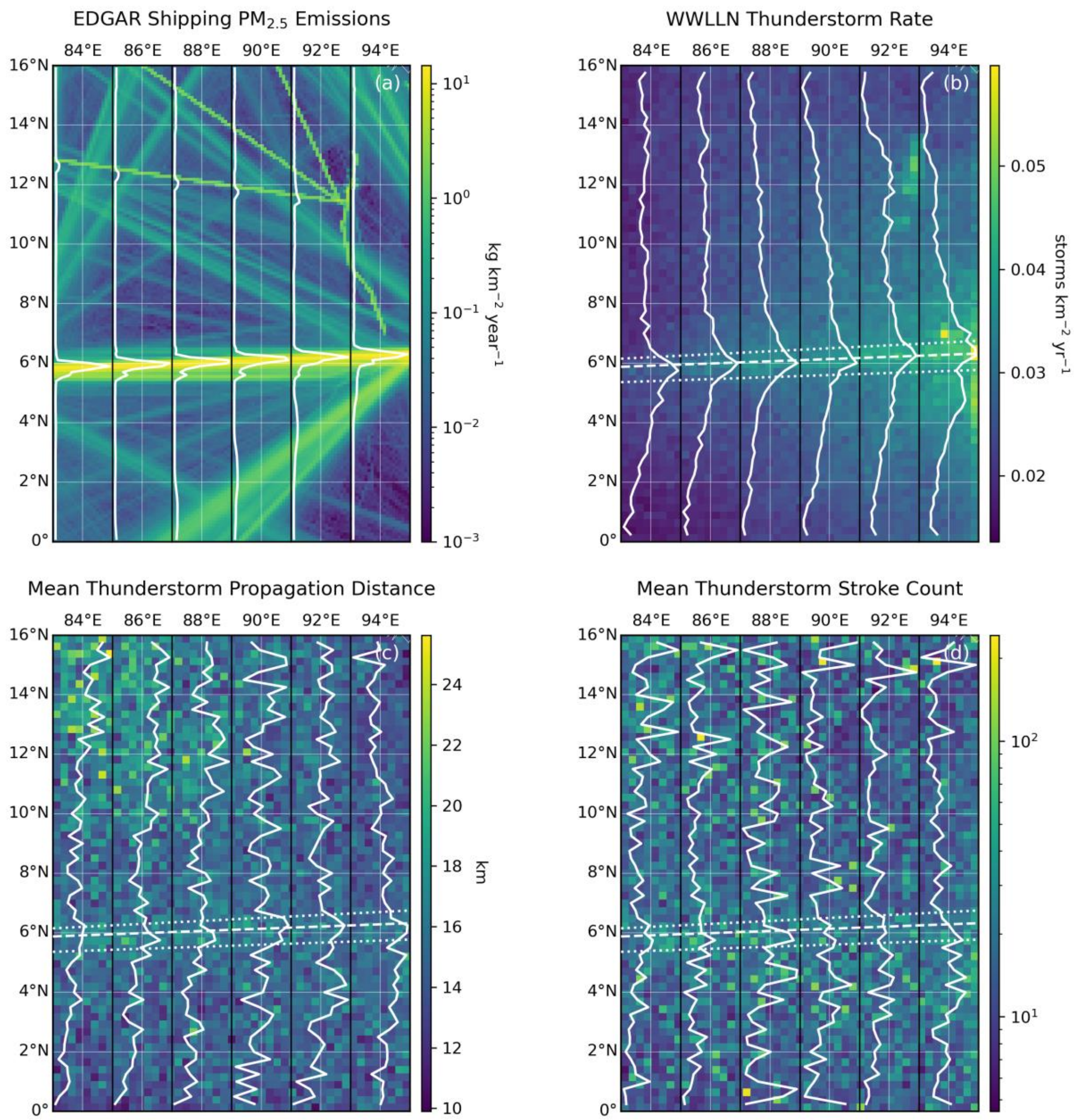

Figure 2. Regional distributions of (a) EDGAR $PM_{2.5}$ shipping emissions, (b) WWLLN thunderstorm area rates, (c) mean WWLLN thunderstorm propagation distances, and (d) mean WWLLN thunderstorm stroke counts over the Bay of Bengal shipping lane. For each longitude bin (black lines), the signal variation by latitude is depicted with a white line overlay. The peak (dashed) and 10th percentile width (dotted) of the shipping lane are also mapped in b-d by fitting the primary EDGAR emissions signature across longitude bins in (a) to a linear model.

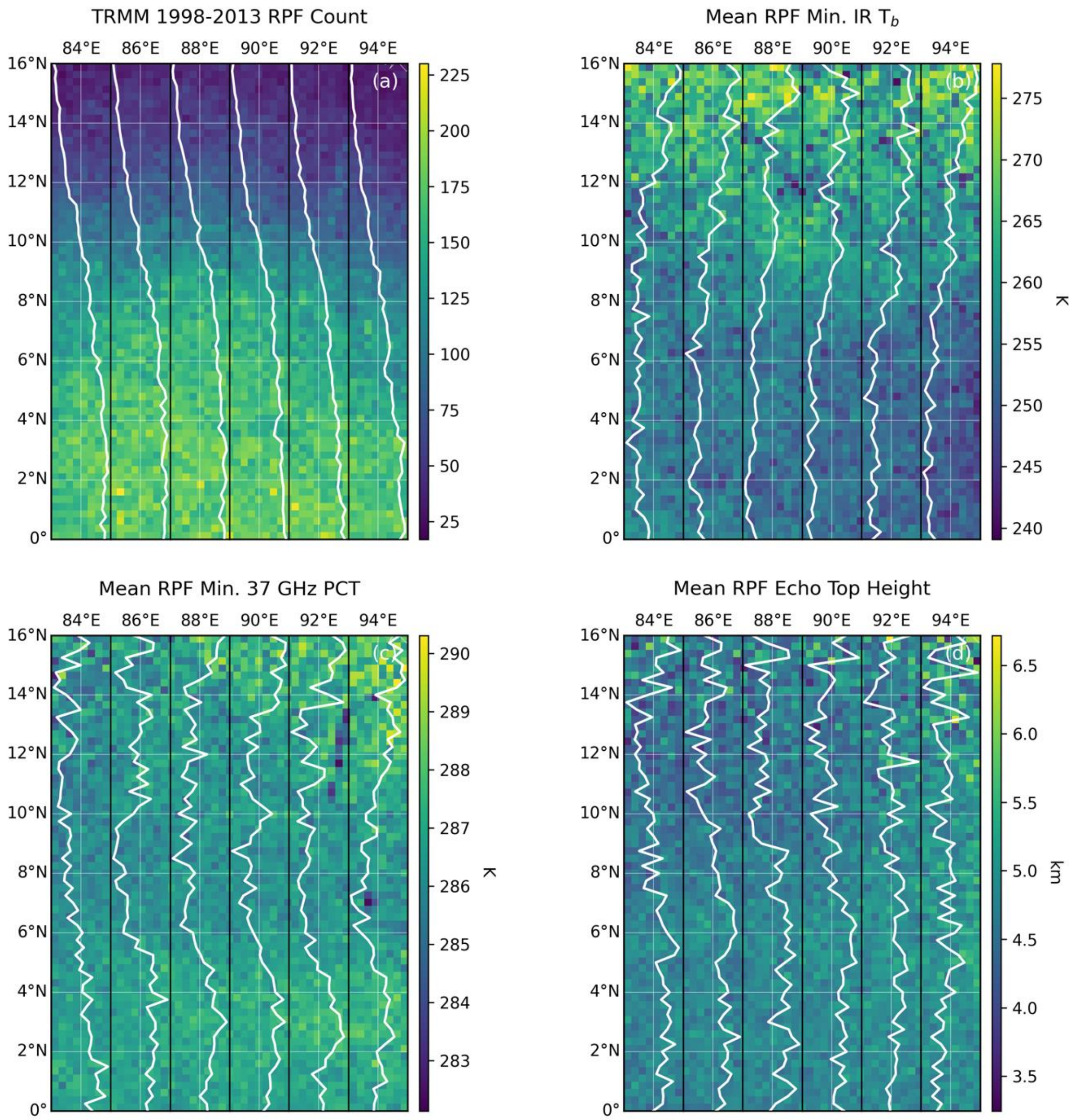

Figure 3. As in Figure 2, regional plots showing TRMM RPF (a) storm counts, and mean microphysical parameters including (b) minimum 10.8μm infrared brightness temperatures, (c) minimum passive microwave 37 GHz PCTs, and (d) PR echo top heights over the Bay of Bengal region during the northern hemisphere winter season.

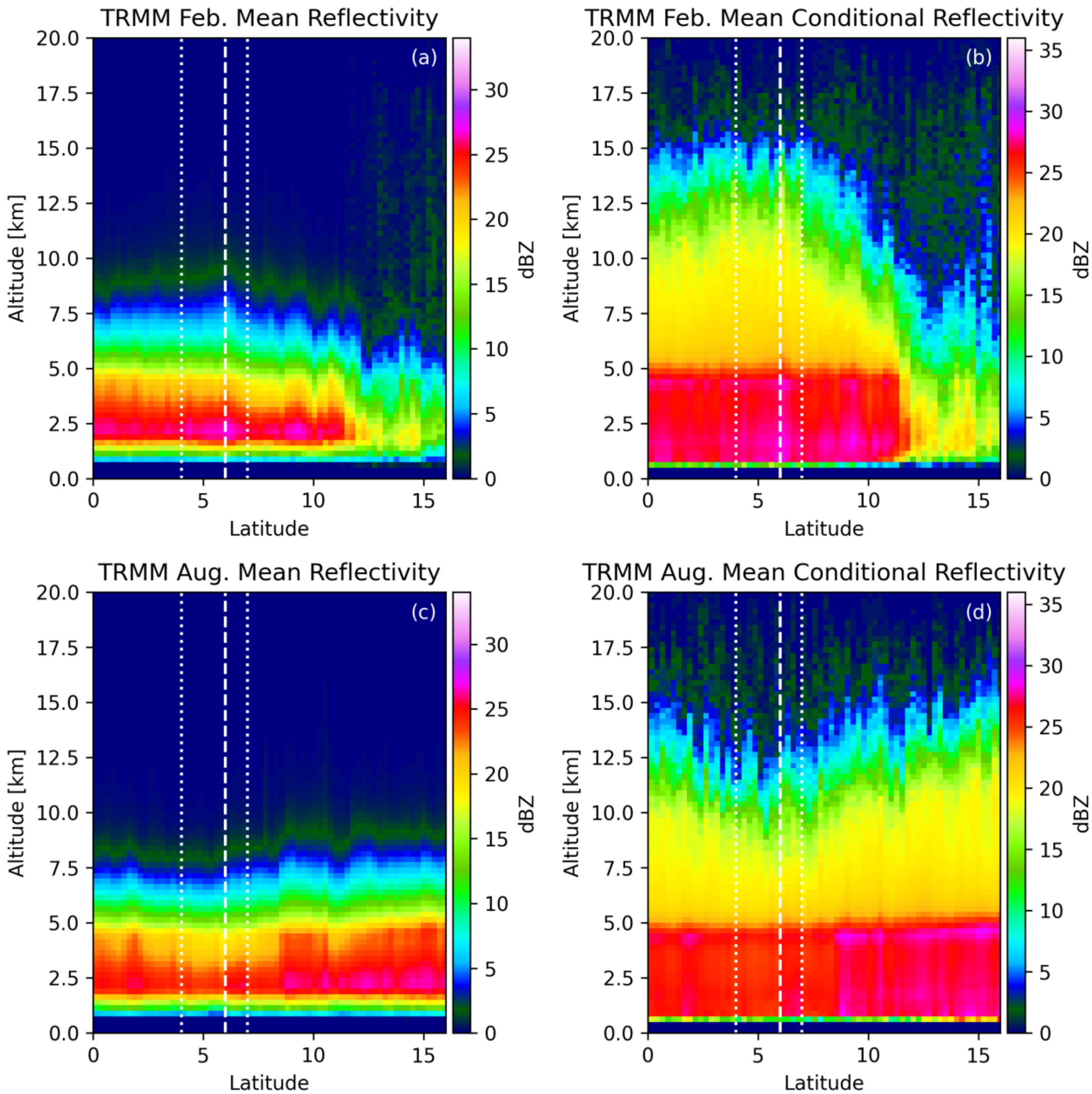

Figure 4. TRMM PR raining pixel vertical reflectivity profiles over the Bay of Bengal region from Figures 2 and 3 at the (a-b) February and (c-d) August extremes of the local seasonal cycle. Average reflectivity profiles from all raining pixels in each latitude bin are shown in (a) and (c). Conditional reflectivity profiles from only raining pixels with echoes exceeding each altitude are shown in (b) and (d). The ship track is represented via the overall peak (dashed) and 10th percentile width (dotted) from the EDGAR emissions data with white vertical lines in each panel.

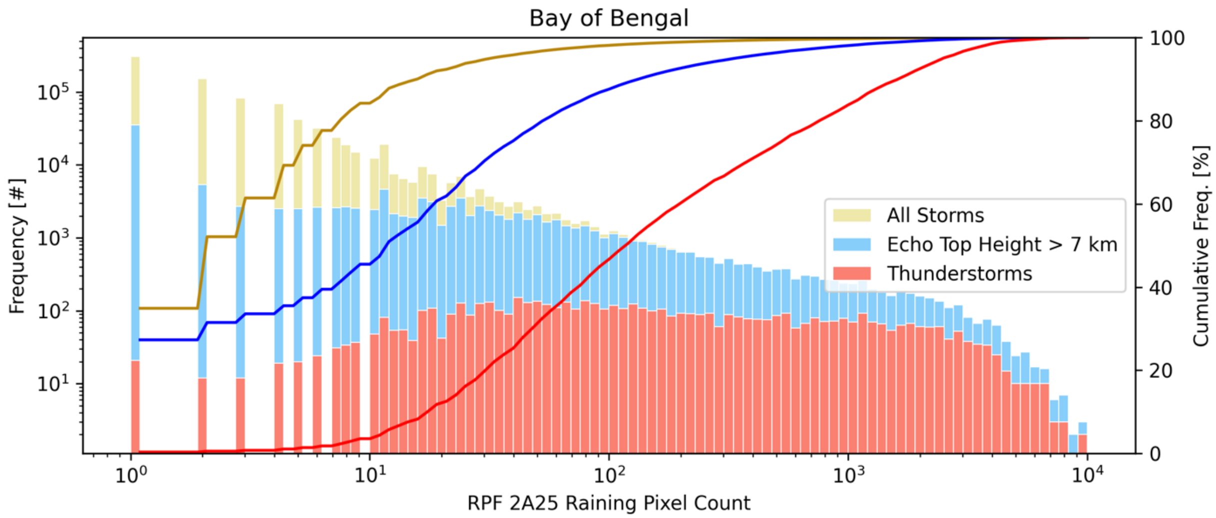

Figure 5. Distributions of TRMM RPF 2A25 raining pixel counts for all storms, tall storms, and thunderstorms over the Bay of Bengal region from Figures 2-4.

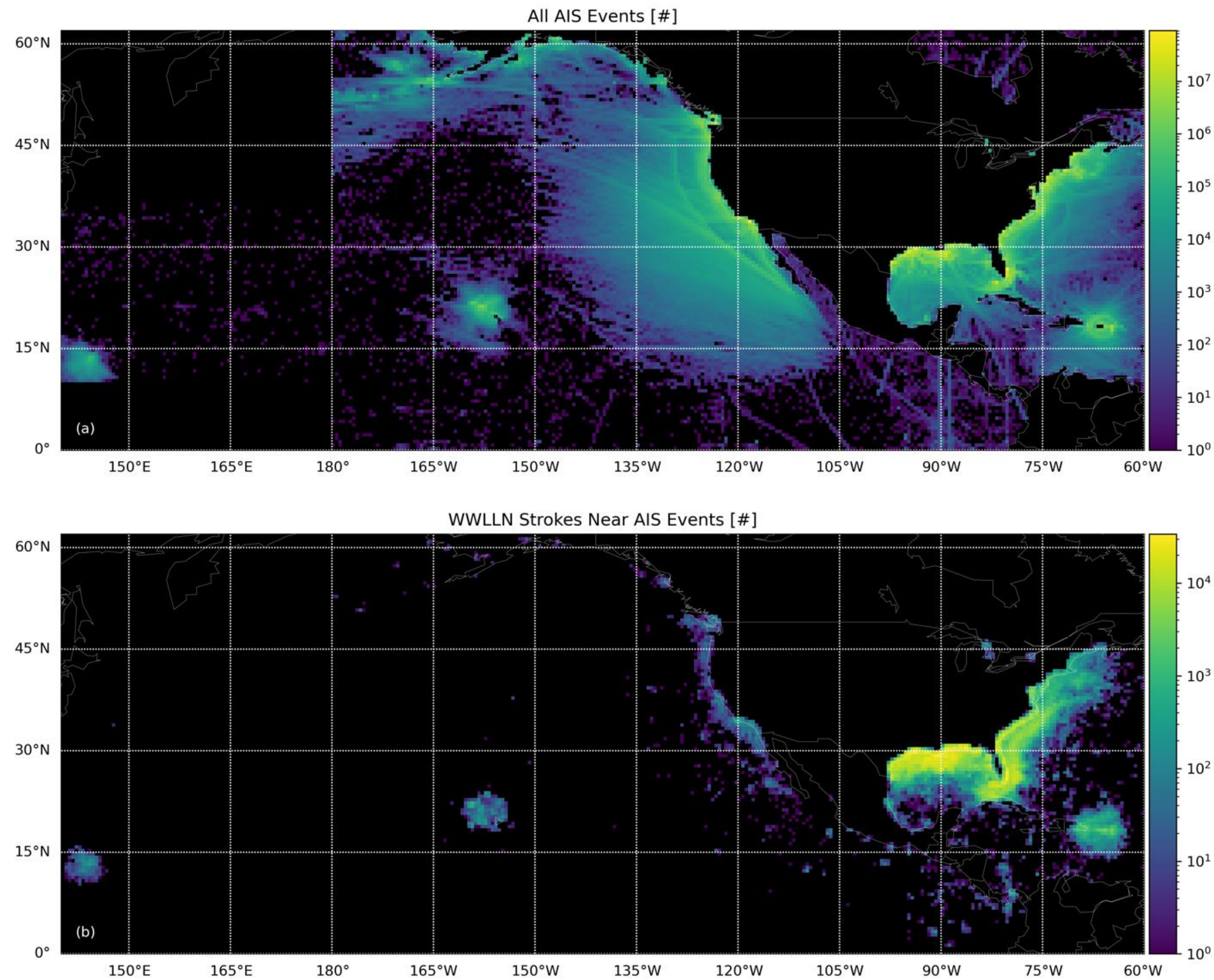

Figure 6. Distributions of (a) all AIS events in the NOAA dataset and (b) WWLLN strokes that are matched to AIS events. The western, southern, and eastern boundaries of the maps reflect the boundaries of the AIS data domain, while the discontinuity at the date line is an artifact in the NOAA data.

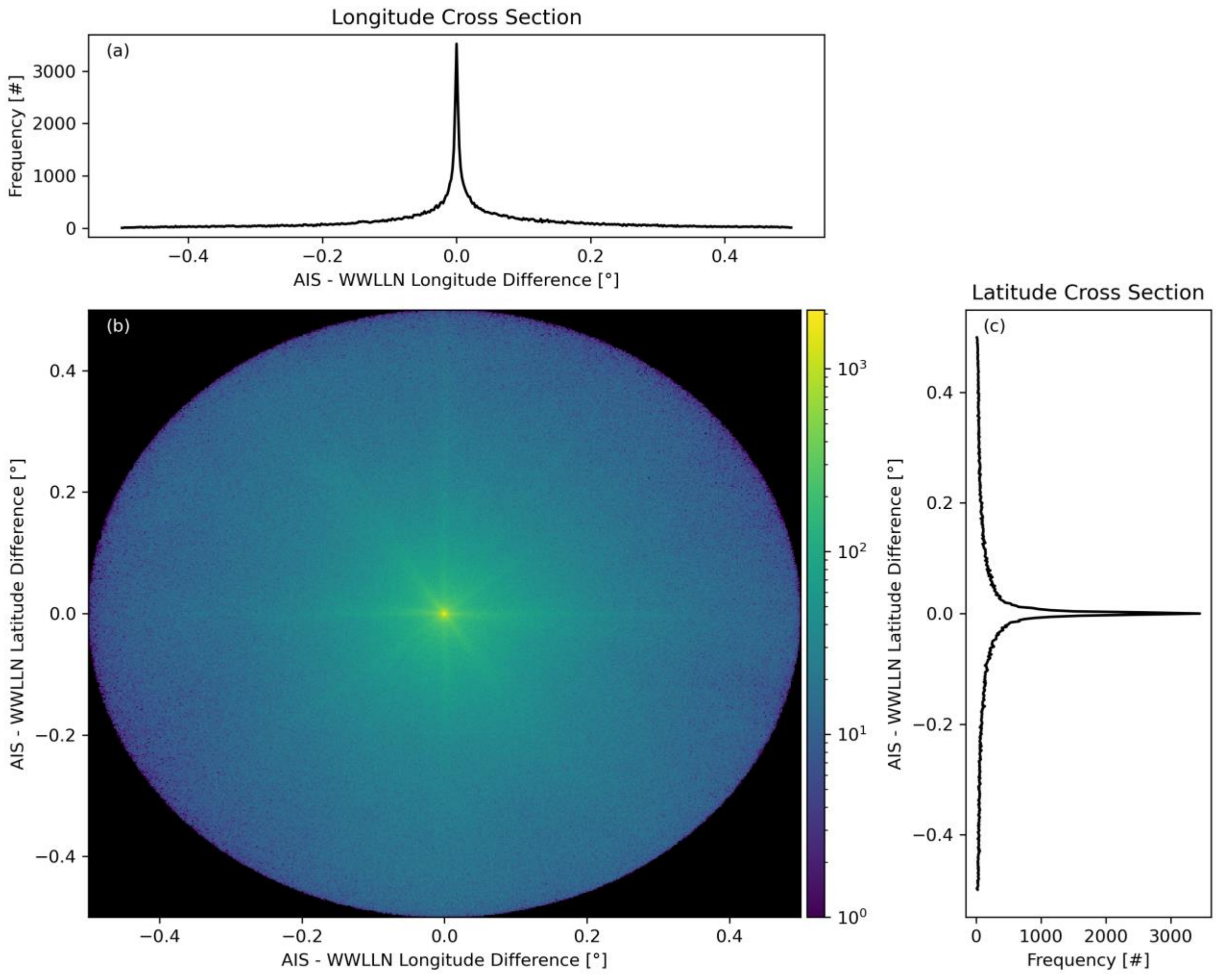

Figure 7. Distributions of WWLLN stroke locations matched to AIS events relative to the ship position at the point (0,0). (a) Longitude cross section through the center of the domain. (b) Two-dimensional histogram of WWLLN strokes. (c) Latitude cross section through the domain center.

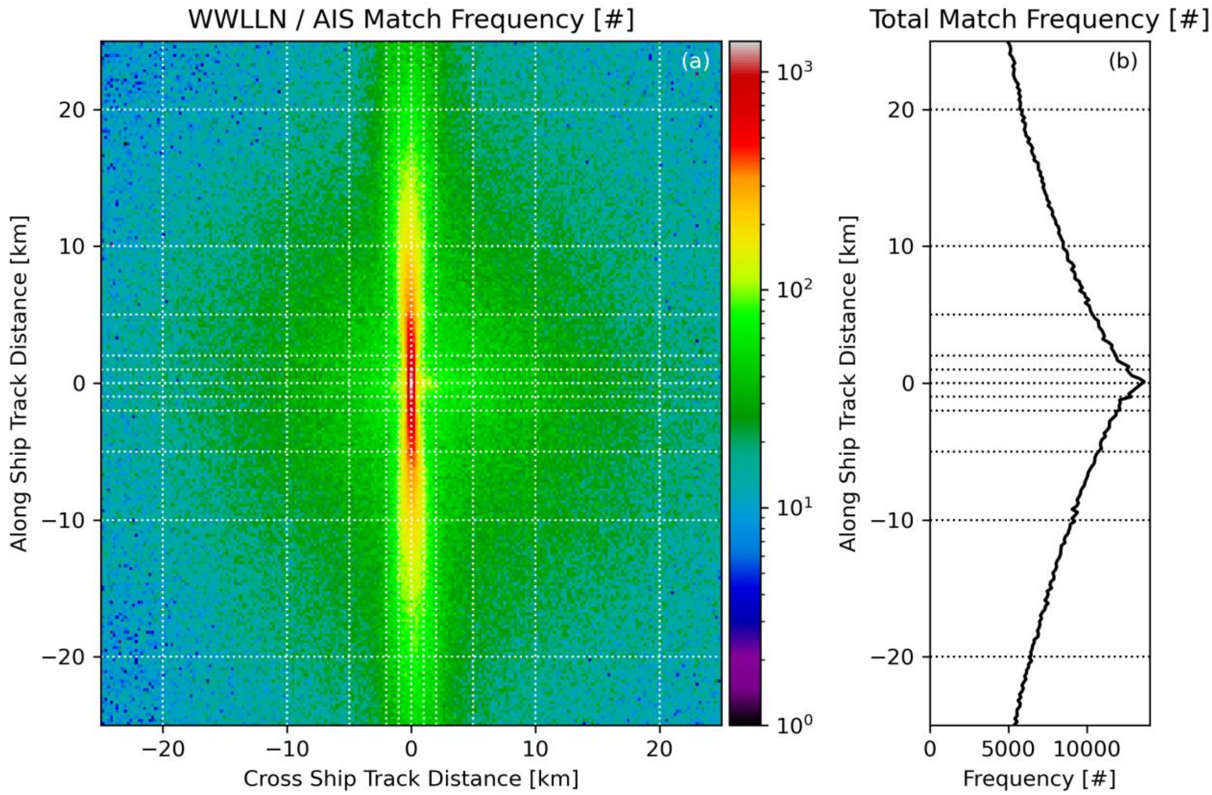

Figure 8. As in Figure 7, the locations of WWLLN strokes surrounding the matched ship, but with the coordinate system rotated to reflect the vessel heading. The two-dimensional histogram of stroke displacements is quantified in (a) using along-track and cross-track distances, with the ship motion towards the top of the figure. Total stroke counts along the ship course are shown in (b). Dotted lines depict 0, 1, 2, 5, 10, and 20 km displacements in each direction from the ship position.

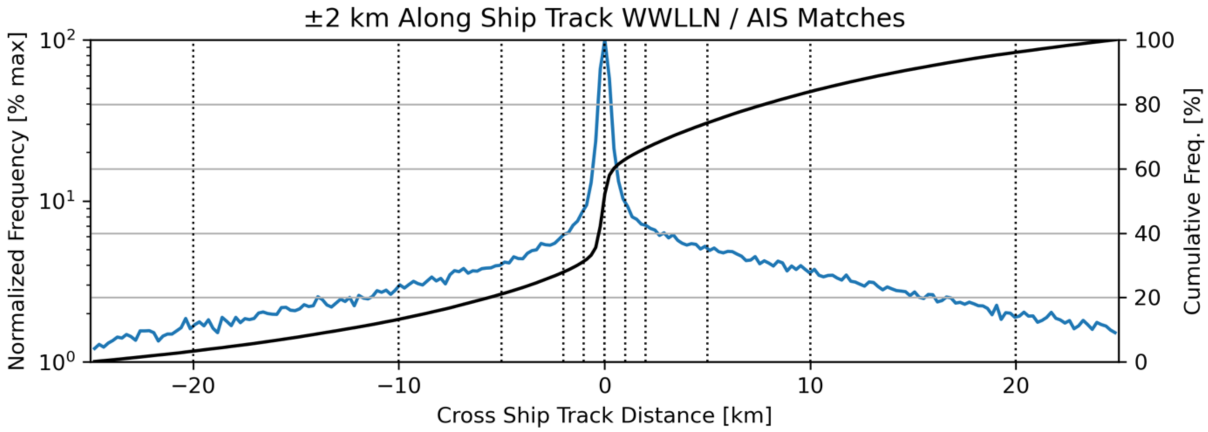

Figure 9. Cross-track distribution of WWLLN stroke counts for all strokes within 2 km of the ship position in the along-track direction. Stroke frequencies are normalized as a percent of the maximum. The CDF is also overlaid in black.

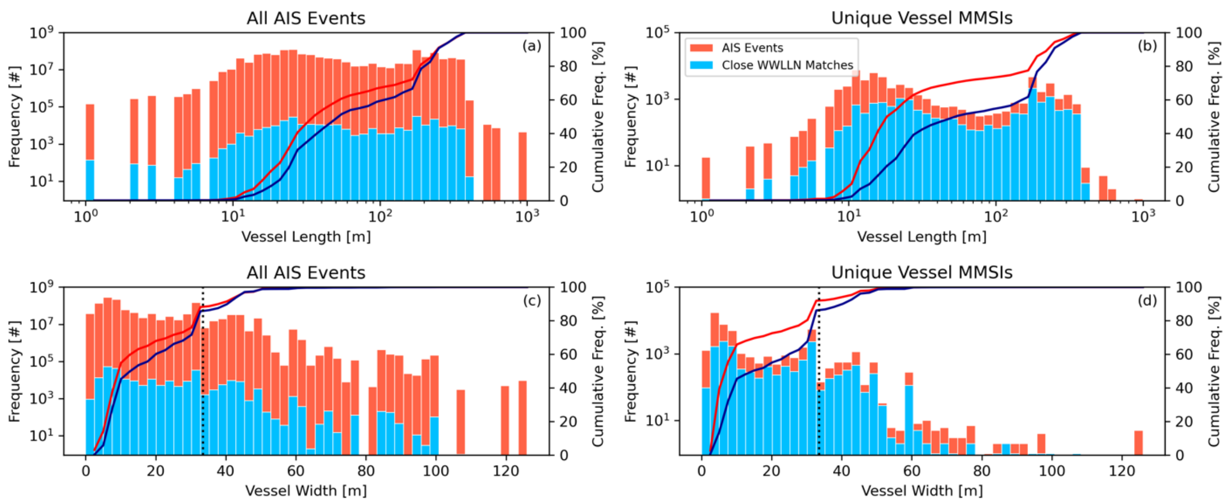

Figure 10. Distributions of (a,c) AIS events, and (b,d) unique vessels in the NOAA AIS dataset by (a-b) vessel length and (c-d) vessel width. Separate distributions and CDFs are shown for all AIS events (red) and close (i.e., within 2-km) WWLLN-matched AIS events (blue). The maximum vessel width for transiting the Panama Canal (i.e., PANAMAX) is indicated with a vertical dotted line in (c-d).

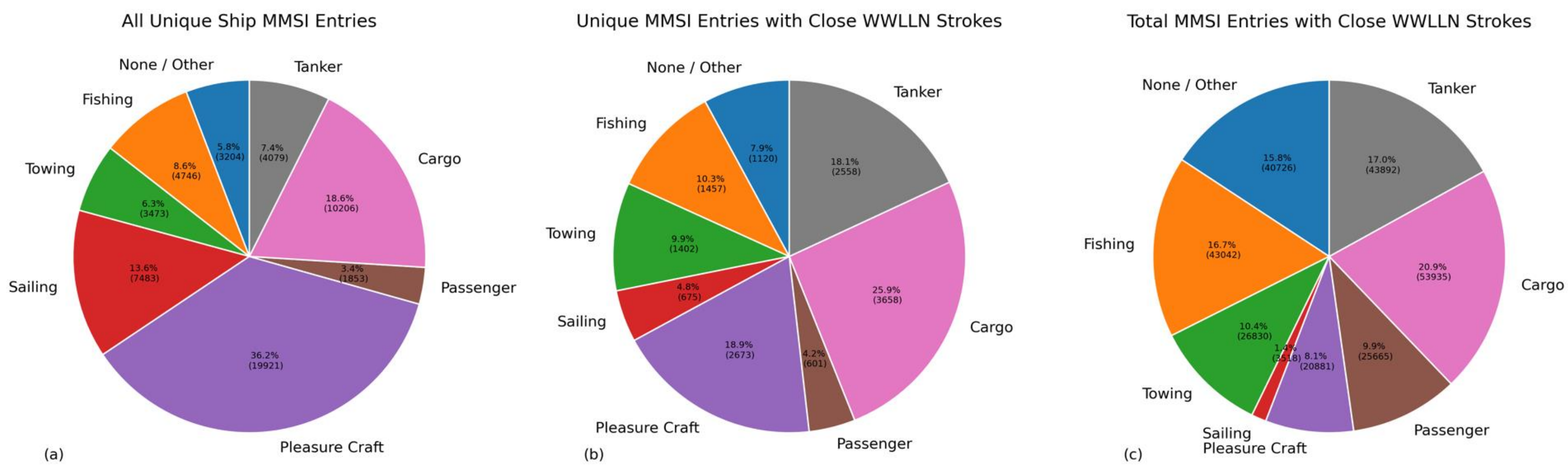

Figure 11. Pie charts showing the frequency of (a) all unique vessels in the NOAA dataset, (b) unique vessels with close WWLLN matches, and (c) all close WWLLN matches in 8 distinct categories of maritime traffic.

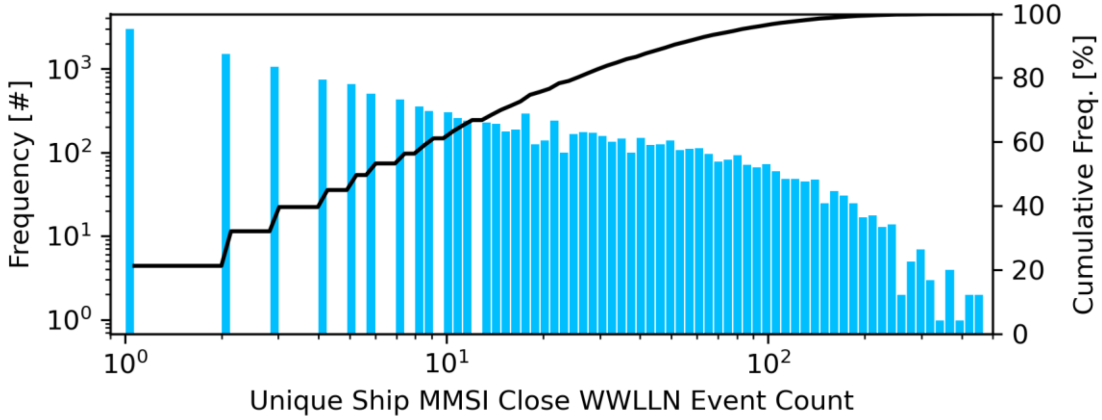

Figure 12. Histogram and CDF of the number of close WWLLN matches on each unique vessel that has had a close lightning encounter.

AGU PUBLICATIONS

Earth and Space Science

Supporting Information for

Interactions between Lightning and Ship Traffic

Michael Peterson[1]

[1] ISR-2, Los Alamos National Laboratory, Los Alamos, New Mexico

Contents of this file

Figures S1 and S2

Introduction

Figures S1 to S2 replicate Figures 1 and 3 to better show the full dataset – not just the regions / season that we are highlighting. Figure S1 allows does not restrict the logarithmic color scaling, as in Figure 1, and thus shows the upper and lower boundaries of WWLLN stroke densities across the globe. Figure S2, meanwhile, shows the average TRMM RPF properties from Figure 3 over the full year rather than just the northern hemisphere winter months.

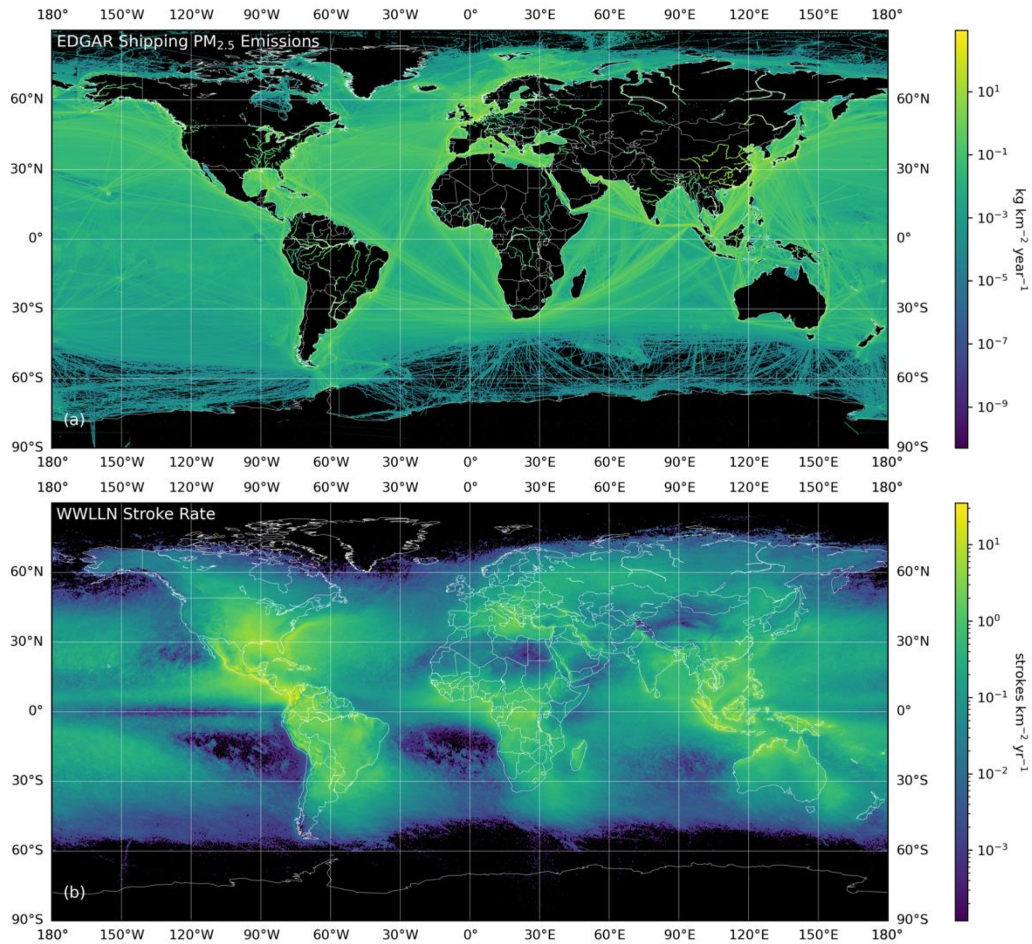

Figure S1. Global distributions of the annual average (a) EDGAR $PM_{2.5}$ shipping emissions and (b) WWLLN stroke rates.

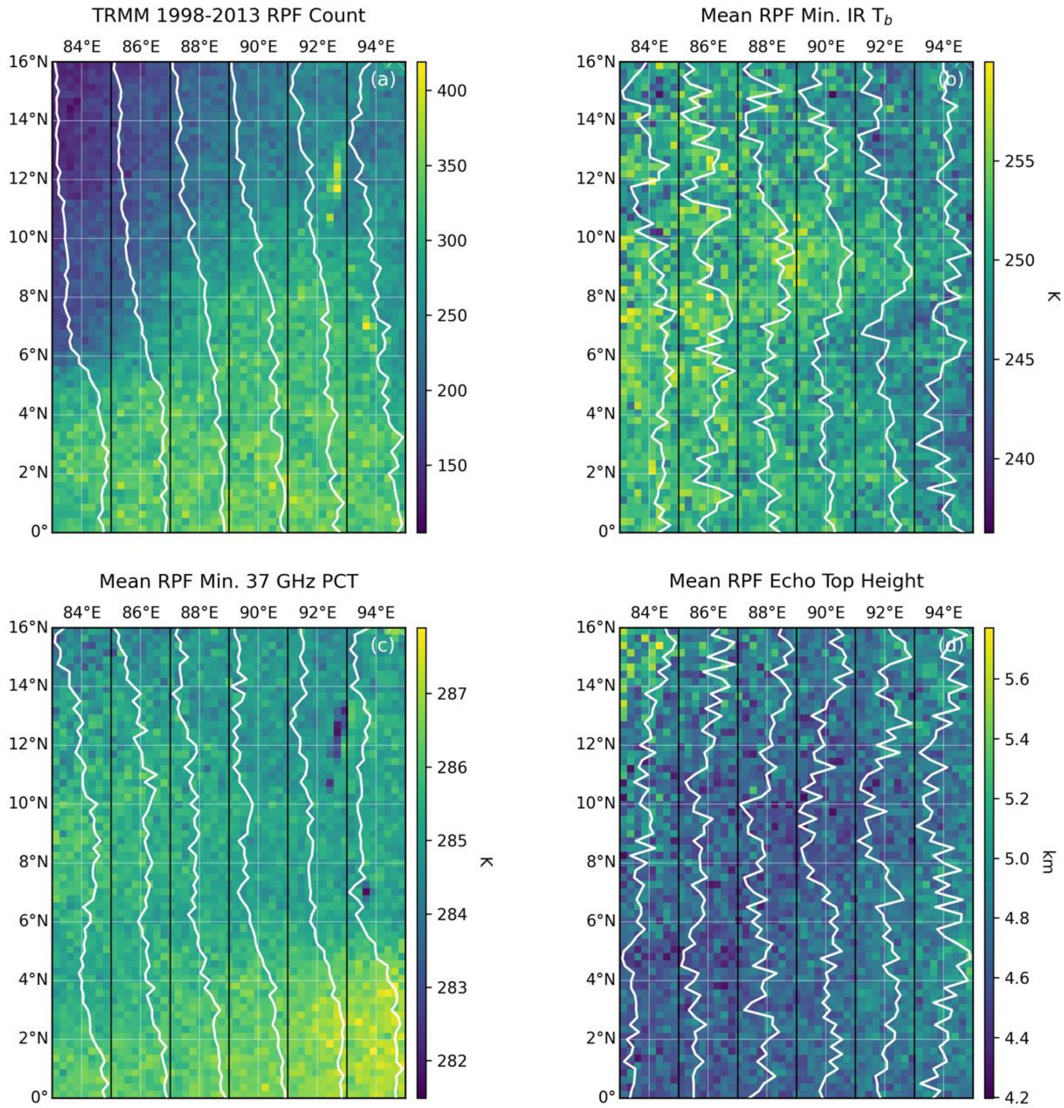

Figure S2. As in Figure 3, regional plots showing TRMM RPF (a) storm counts, and mean microphysical parameters including (b) minimum 10.8μm infrared brightness temperatures, (c) minimum passive microwave 37 GHz PCTs, and (d) PR echo top heights over the Bay of Bengal region during the full year.